Journal of Sound and Vibration (1999) **225**(2), 239–282
Article No. jsvi.1998.2256, available online at http://www.idealibrary.com on IDEAL®

STRUCTURE-BORNE SOUND POWER AND SOURCE CHARACTERIZATION IN MULTI-POINT-CONNECTED SYSTEMS. PART 3: FORCE RATIO ESTIMATES

R. A. FULFORD† AND B. M. GIBBS

Acoustics Research Unit, University of Liverpool, L69 3BX, England

(*Received* 11 *November* 1997, *and in final form* 12 *October* 1998)

A fundamental problem in the field of structure-borne sound is the characterization of dynamic sources with respect to vibrational power. Though one of the proposed approaches based upon the ability of a source to deliver power is promising, it necessitates estimating the spatial distribution of the forces at the multiple contacts between the source and receiver structure. Hence, by way of both an analytical and a statistical study, in this paper methods are investigated through which the force ratios manifested in a system can be estimated. The analytical study considers methods of estimating the force ratios absolutely whilst the statistical study considers their statistical domain. For the analytical study all attempts in estimating failed under the condition of approximately equal point and transfer mobilities. With respect to the statistical part of the study, the mobilities and free velocities in a system are considered as "populations" and grouped functions are introduced to describe their distributions. Based upon these grouped functions, simple expressions are derived for the statistical distribution of the force ratios. A generalized approach is used throughout so that the work is applicable to many systems.

1. INTRODUCTION

In a previous paper by Fulford and Gibbs [1], the characterization of structure-borne sound sources has been re-examined and a suggestion made that the approach based upon the work of Mondot and Peterson [2] warrants further study. The promise of their approach is that the source characterization is determined with respect to the sources ability to deliver power rather than to the power delivered. This circumvents the fundamental problem that, due to strong dynamic structural coupling, the power delivered is dependent upon both the source and receiver structures. Two functions are introduced; the source descriptor and the coupling function. The former describes the sources ability to deliver the power while the latter represents a filter determining how much of this power is manifested. Together, as a product, the two functions establish the power delivered.

†Present address: Institute für Technische Akustik, T.U. Berlin, 10587 Berlin, Germany

0022-460X/99/320239 + 44 $30.00/0

Although considered promising, the formulation does suffer in that where the structural coupling involves multiple points [1] (and/or multiple degrees of freedom†) both the source descriptor and coupling function can be calculated only if the force distribution amongst the contact point is known: i.e.,

$$S_i^n = (V_{sfi}^n)^2/2Y_{sii}^{nn\Sigma *}, \qquad Cf_i^n = Y_{sii}^{nn\Sigma *} Y_{rii}^{nn\Sigma}/|Y_{sii}^{nn\Sigma *} + Y_{rii}^{nn\Sigma *}|^2, \tag{1, 2}$$

where

$$Y_{ii}^{nn\Sigma} = \sum_{m=1}^{N} \sum_{j=1}^{6} Y_{ij}^{mn} F_j^m/F_i^n. \tag{3}$$

The "scale" of the problem is illustrated whence the forces in a system are related to the structural properties and the free velocities,

$$[F] = [Y_s + Y_r]^{-1}[V_{sf}], \tag{4}$$

the dimension of the equation set being MN, where N is the number of contact points and M the number of degrees of freedom. It can be seen that the number of mobility and free velocity terms needed to be obtained prior to a calculation of the forces ensures that the formulation quickly becomes impractical. Moreover, the forces are seen to depend upon both the source and receiver structural properties so that any use of equation (4) means the hoped for (receiver) independence of the source descriptor function is compromised. (A list of symbols is given in the Appendix A).

A small "glimmer of hope" comes from the formulation upon the realization that it is not forces themselves which are involved with the source descriptor and coupling function formulation but the distribution of these forces: i.e., the force ratios in the system. The hope is then that these distributions are less sensitive to structural variations than the forces themselves. Thus it is hypothesized that it may be possible to assume or estimate them in some manner.

In their initial study [1], the authors used simple estimates of force ratios to calculate the transmitted power in connected beam structures and compared these results with those of the exact transmitted power. Whilst the results were promising, a conclusion from the work was that further attention should be given to those parameters which determine the force ratios; namely the source and receiver mobilities and the source free velocities, see equation (4). This was undertaken in a second paper by the authors [3] where it was attempted to establish generalized relationships amongst the parameters for each of the mass, stiffness, and resonant-controlled regions which can be expected for a structure. Though the attempt was only partially successful, adequate results were procured to allow this follow-on study to be likewise generalized and thus not restricted to specific "named" systems.

Hence, in this paper, methods of estimating the force ratios in multi-point-connected source–receiver systems are considered. An analytical study is first conducted, followed by a statistical study.

†As used in this paper, the term degrees of freedom refers to directional components, i.e. tanslational (x, y, z) and rotational (ϕ_x, ϕ_y, ϕ_z).

The investigation is limited to the simplified but nonetheless important case in which only translational forces act and wherein only four contact points exist. Though it is acknowledged that moment-induced power can be of equal importance [4], this simplified model was adopted to allow the development of a methodology. However, the "moment problem" was always "kept in mind" allowing the developed methodology to take into account such a criterion at a later stage.

2. ANALYTICAL STUDY

While equation (4) shows that the forces at the contacts between the source and receiver are dependent upon both structures, it also reveals that for a system with structures of greatly differing mobility trends the forces will be dominated by the structure with the largest mobility magnitude. Where the source mobilities are large compared to those of the receiver, its structure can therefore, with respect to an approximate calculation of the forces, be ignored. Moreover, such an assumption can be realistic for building engineering where the machine mobilities are often of order 10^2 greater than those of a thick concrete floor (commonly of order 10^{-5} m/Ns [5]).

For source characterization such a constant force source† (CFS) assumption is of clear interest, since when invoked, the problem of the forces being dependent upon both the source and receiver is removed. To simplify the study, a CFS is therefore assumed for the analytical study. The general case where the receiver structure also influences the force ratios, i.e., the matched situation, is revisited and considered in the statistical analysis.

2.1. ESTIMATE OF FORCE RATIO BY ITERATION

An exact calculation of the force ratios based upon equation (4) involves acquisition of all the mobility terms, formation of the mobility matrix and then inversion of this matrix. As an alternative (because the equation is in essence only a set of MN linear equations) an approximate solution can be obtained by using the method of iteration. If convergence is rapid and the forthcoming solution, accurate with respect to engineering limits, the method has the advantage that it is computationally more efficient than a complete matrix inversion. Moreover, a study based upon an iterative scheme is useful because if the initial approximations to the solution are based upon the diagonal elements of the matrix, i.e., the point mobilities, the influence upon the solution of the off-diagonal elements, i.e., the transfer mobilities, is revealed. Rapid convergence for example indicates that the transfer mobilities have a limited influence while non-convergence indicates strong influence.

†There may be a possible ambiguity for some readers in the use of the term constant force source. In the paper this simply refers to situations where the receiver mobilities do not influence the force ratios, i.e. it does not purport to the case where the force distribution is constant for all points.

Three fictive sources were considered; see Figures 1–3. Source A was mass controlled with high I_{yy} and low I_{xx} subjected to translational excitation, source B the same structure but subjected to rotational excitation about the y-axis and source C was a resonant controlled structure. The characteristic of mass, stiffness and resonance, determined in the author's earlier paper, was utilized [3].

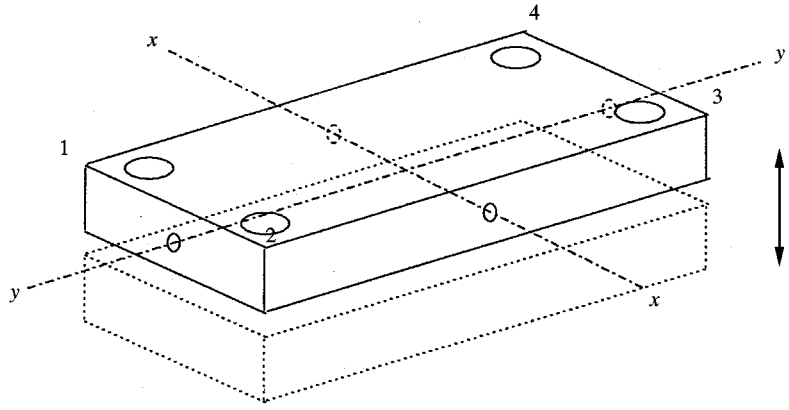

Figure 1. Mass-controlled behaviour of a source with high I_{yy} and low I_{xx} and translational excitation.

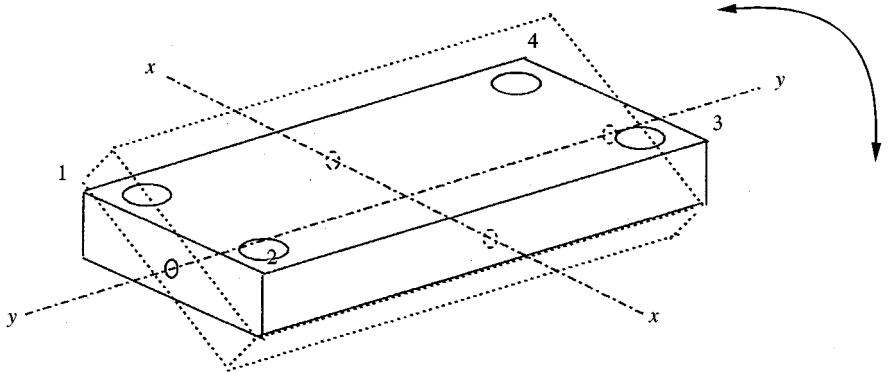

Figure 2. Mass-controlled behaviour of a source with high I_{yy} and low I_{xx} and rotational excitation about the y-axis.

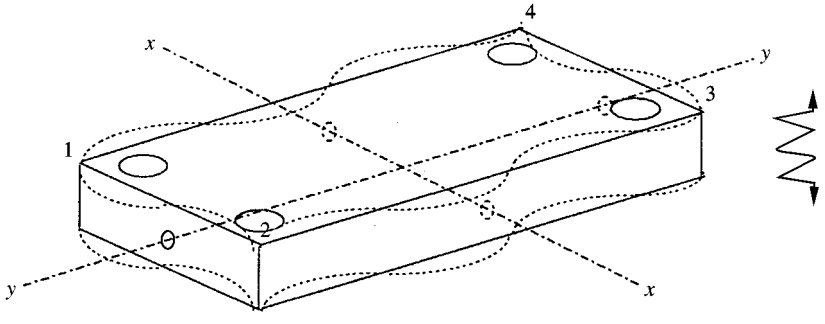

Figure 3. A source with resonance-controlled behaviour.

Upon the introduction of fictive sources, a methodology was devised through which the mobilities and free velocities could be described and the influence of the off-diagonal mobility terms could be assessed.

Initially, to reduce the number of independent parameters, all of the point mobilities and all of the free velocities were assigned equal magnitude. Later a range within which the transfer mobility magnitude could exist was defined and the individual mobility values assigned at random from within it. For the study, the range was defined as $10^{(n-1)/10} < |Y^{tr}| \leqslant 10^{n/10}$ where $n = 1, 2, \ldots, 10$. This meant that for each source, 10 different mobility conditions were considered. As regards the phase of the parameters, this was determined in accordance with the authors' earlier paper [3] wherein for source A,

$$\theta\{Y^{12}\} = \theta\{Y^{34}\} = \theta\{Y^{11}\} = \theta\{Y^{22}\} = \theta\{Y^{33}\} = \theta\{Y^{44}\} = -\pi/2, \tag{5}$$

$$\theta\{Y^{13}\} = \theta\{Y^{14}\} = \theta\{Y^{23}\} = \theta\{Y^{24}\} = \pi/2, \theta\{V_{sf}^{1}\} = \theta\{V_{sf}^{2}\}$$

$$= \theta\{V_{sf}^{3}\} = \theta\{V_{sf}^{4}\} = 0, \tag{6, 7}$$

for source B,

$$\theta\{V_{sf}^{1}\} = \theta\{V_{sf}^{4}\} = 0, \qquad \theta\{V_{sf}^{2}\} = \theta\{V_{sf}^{3}\} = \pi, \tag{8, 9}$$

whilst for source C,

$$\theta\{Y^{mn}\} = \theta\{V_{sf}^{n}\} = random. \tag{10}$$

In the format of an Argand diagram, the parameter fields are illustrated in Figures 4–6.

Three iteration techniques were considered of which the Gauss–Jacobi and the Gauss–Seidel techniques have a mathematical history [6], while the other was based upon the effective point mobility, where the updated force was obtained via an updated calculation of the effective mobilities,

$$F_{(it+1)}^{n} = V_{sf}^{n} / Y_{s(it)}^{nn\Sigma}, \tag{11}$$

where *it* is the iteration number.

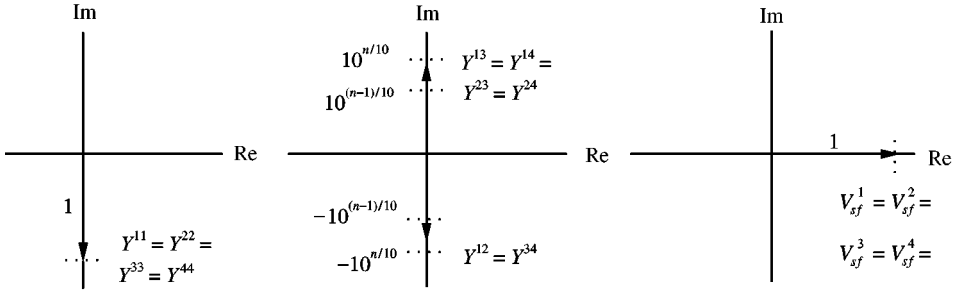

Figure 4. Using an Argand diagram format, the (a) point mobilities, (b) transfer mobilities and (c) free velocities of a mass-controlled source with high I_{yy} and low I_{xx} and translational excitation about the y-axis.

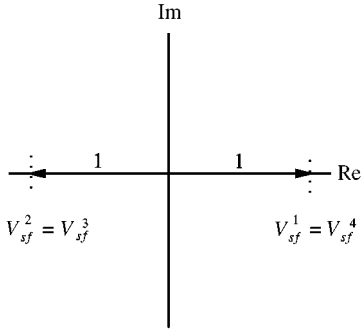

Figure 5. Using an Argand diagram format, the free velocities for rotational excitation.

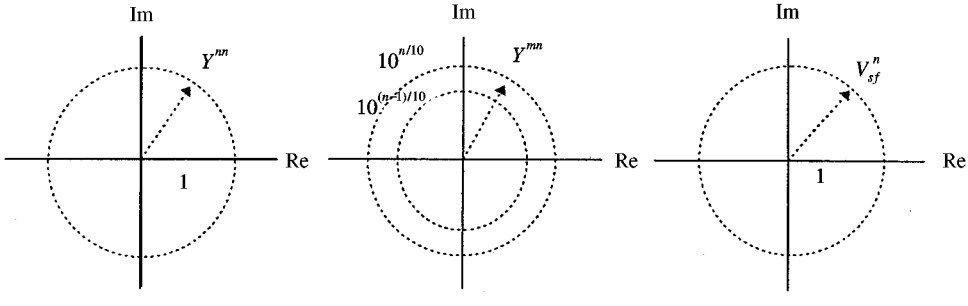

Figure 6. Using an Argand diagram format, the (a) point mobilities. (b) transfer mobilities and (c) free velocities of a resonance-controlled source..

In all cases, the initial estimate of the force was the quotient of the free velocity and source point mobility,

$$F^n = V_{sf}^n / Y^{nn}, \tag{12}$$

which, in accordance with the ideals of the study, involves only the leading diagonal of the mobility matrix.

For reasons of brevity, only a selection of the results obtained are shown,

For source B, the normalized estimates of the magnitude of F^2/F^1 resultant from the effective point mobility iteration scheme is shown in Figure 7. Each line-type represents a different range from which the magnitude of the transfer mobilities were selected. It is suggested that only rapid and accurate convergence is apparent for Y^{tr}/Y^{pt} ranges of $\{10^{0\cdot3}, 10^{0\cdot4}\}$ and below. For the other ranges there is either non-convergence or large discrepancies.

The Gauss–Jacobi method was more promising, where the estimates were found to converge quickly to the true value for the Y^{tr}/Y^{pt} ranges of $\{10^{0\cdot6}, 10^{0\cdot7}\}$ and below. However, for higher ranges the estimate either converged to an incorrect value or did not converge at all. The Gauss–Seidel method was most favourable though, in that, the estimates converged to the true value for all Y^{tr}/Y^{pt} ranges except for the extreme case of $Y^{tr} \approx Y^{pt}$.

Similar results were seen for source A.

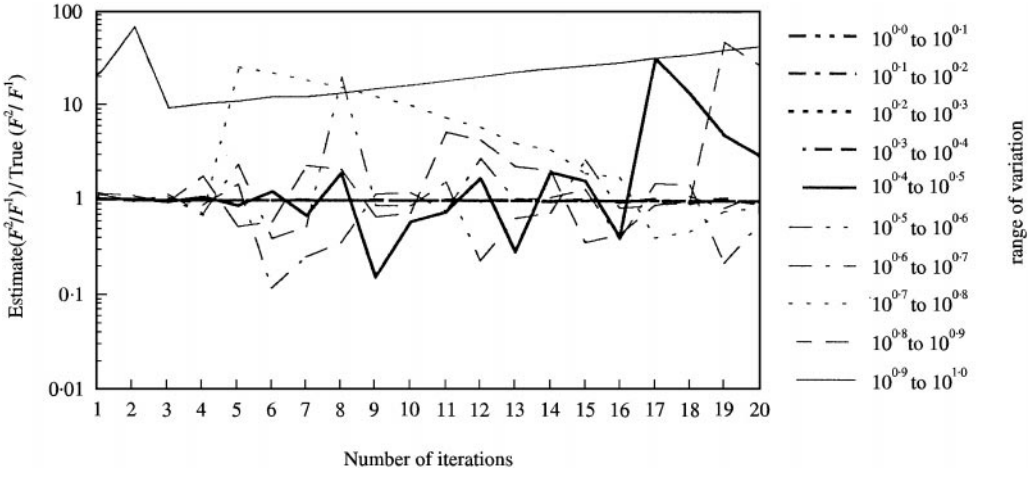

Figure 7. Effective mobility iteration for mass-controlled source with high I_{yy} and low I_{xx} and rotational excitation about the y-axis.

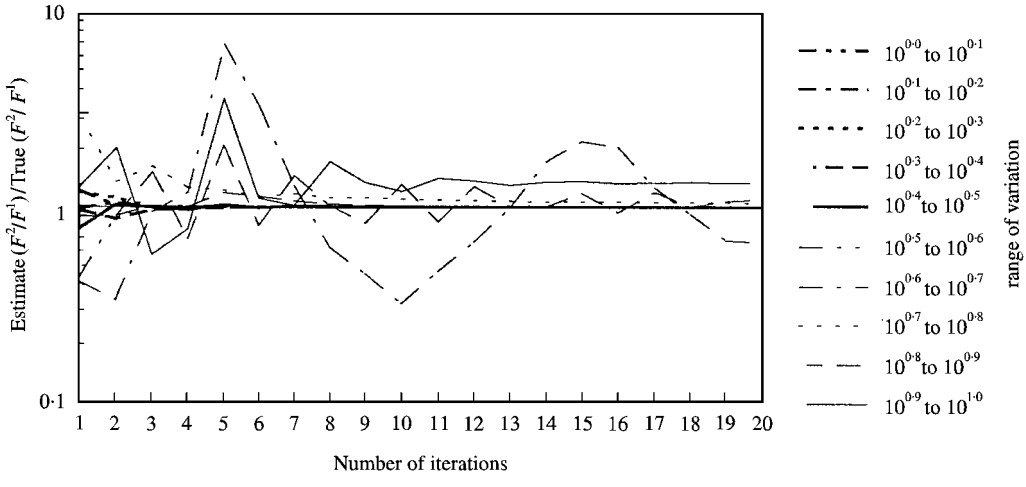

Figure 8. Convergence of magnitude for Gauss–Jacobi iteration applied to a resonance-controlled source.

Since for a mass-controlled source, the phase of the mobilities and free velocities is discretized, it can be deduced that the phase of the force ratios is likewise discrete and hence its convergence for this source type need not be considered. For a resonance-controlled source, the phases of the mobilities and free velocities are however variable whereupon the phases of the force ratios are also random. For this source type, the convergence of both magnitude and phase is therefore of interest. Hence, for where the Gauss–Jacobi iteration scheme applied to source C, the magnitude of F^2/F^1 is as shown in Figure 8 and for application of the Gauss–Seidel scheme the phase of F^2/F^1 is as shown in Figure 9.

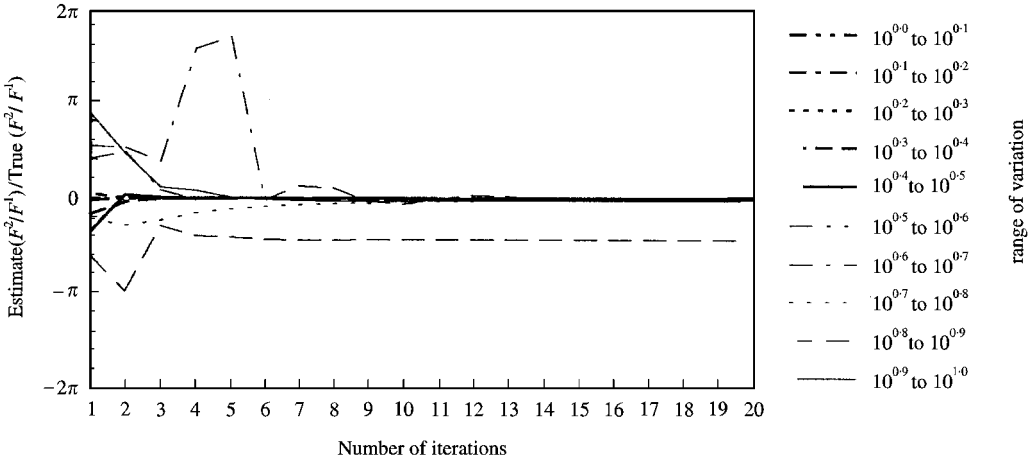

Figure 9. Convergence of phase for Gauss–Seidel iteration applied to a resonance-controlled source.

The estimate of the magnitude is seen to converge towards the true for all Y^{tr}/Y^{pt} ranges of $\{10^{0.5}, 10^{0.6}\}$ and below. This is very similar to that observed for the mass-controlled sources; hence it is suggested that the condition for non-convergence is similar for all three source types.

As regards Figure 9, the phase estimate is seen to be accurate only for Y^{tr}/Y^{pt} ranges of $\{10^{0.5}, 10^{0.6}\}$ and below. Clearly, this is in contrast to that seen for sources A and B where, for the Gauss–Seidel method the estimate was accurate for all cases except $Y^{tr} \approx Y^{pt}$.

Both the magnitude and phase estimates were accurate for ranges of $\{10^{0.4}, 10^{0.5}\}$ and below, using both the effective point mobility approach and the Gauss–Jacobi approach; successful application of these schemes was therefore similar for all three source types.

2.2. ESTIMATE OF FORCE RATIO BY MATRIX INVERSION

Where the dimension (number of contact points × degrees of freedom) of the system is small, i.e., less than 6, it is mathematically practical to invert the mobility matrix of equation (4) and obtain closed-form expressions for the true forces. Upon doing so for the four contact point system, the expression for F^1 normalized by the determinant of the mobility matrix is

$$F^1_{norm} = V^1_{sf}\left(\frac{1}{Y^{11}} - \frac{Y^{34}Y^{43}}{Y^{11}Y^{33}Y^{44}} - \frac{Y^{23}Y^{32}}{Y^{11}Y^{22}Y^{33}} - \frac{Y^{24}Y^{42}}{Y^{11}Y^{22}Y^{44}} + \frac{Y^{23}Y^{34}Y^{42}}{Y^{11}Y^{22}Y^{33}Y^{44}} + \frac{Y^{24}Y^{32}Y^{43}}{Y^{11}Y^{22}Y^{33}Y^{44}}\right)$$

$$+ V_{sf}^2 \left(- \frac{Y^{12}}{Y^{11}Y^{22}} + \frac{Y^{13}Y^{32}}{Y^{11}Y^{22}Y^{33}} + \frac{Y^{14}Y^{42}}{Y^{11}Y^{22}Y^{44}} + \frac{Y^{12}Y^{34}Y^{43}}{Y^{11}Y^{22}Y^{33}Y^{44}} \right.$$

$$\left. - \frac{Y^{13}Y^{34}Y^{42}}{Y^{11}Y^{22}Y^{33}Y^{44}} - \frac{Y^{14}Y^{32}Y^{43}}{Y^{11}Y^{22}Y^{33}Y^{44}} \right)$$

$$+ V_{sf}^3 \left(- \frac{Y^{13}}{Y^{11}Y^{33}} + \frac{Y^{12}Y^{23}}{Y^{11}Y^{22}Y^{33}} + \frac{Y^{14}Y^{43}}{Y^{11}Y^{33}Y^{44}} - \frac{Y^{12}Y^{24}Y^{43}}{Y^{11}Y^{22}Y^{33}Y^{44}} \right.$$

$$\left. + \frac{Y^{13}Y^{24}Y^{42}}{Y^{11}Y^{22}Y^{33}Y^{44}} - \frac{Y^{14}Y^{23}Y^{42}}{Y^{11}Y^{22}Y^{33}Y^{44}} \right)$$

$$+ V_{sf}^4 \left(- \frac{Y^{14}}{Y^{11}Y^{44}} + \frac{Y^{12}Y^{24}}{Y^{11}Y^{22}Y^{44}} + \frac{Y^{13}Y^{34}}{Y^{11}Y^{33}Y^{44}} - \frac{Y^{12}Y^{23}Y^{34}}{Y^{11}Y^{22}Y^{33}Y^{44}} \right.$$

$$\left. - \frac{Y^{13}Y^{24}Y^{32}}{Y^{11}Y^{22}Y^{33}Y^{44}} + \frac{Y^{14}Y^{23}Y^{32}}{Y^{11}Y^{22}Y^{33}Y^{44}} \right). \tag{13}$$

If the magnitudes of the transfer mobilities are assumed to be small with respect to those of the point mobilities, then those terms involving one transfer mobility in the numerator will be greater than those involving two. In turn, these will be greater than those with three. From this insight, simplified force expressions can therefore be obtained by truncating equation (13) with respect to the number of transfer mobilities in the numerator: i.e., (i) ignoring those terms which have a numerator involving a product of one or more transfer mobilities; (ii) ignoring those terms which have a numerator which involves a product of two or more mobilities; (iii) ignoring only those terms which have a numerator that involves a product of three.

For source B and with respect to an estimate of F^2/F^1, application of these three estimates produces Figure 10. When $Y^{tr} \approx Y^{pt}$ discrepancies can be expected (and

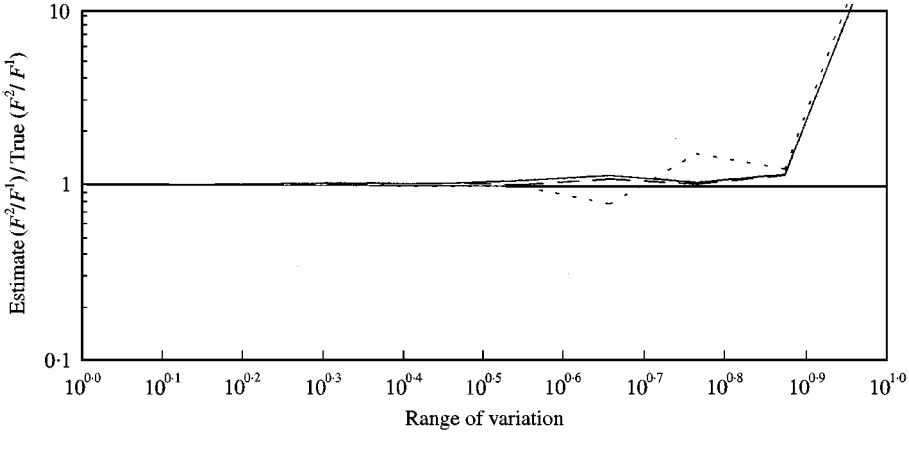

Figure 10. Truncation estimates for mass-controlled source with high I_{yy} and low I_{xx} and rotational excitation about the y-axis. ——, Estimate (i); – – , estimate (ii); - - - - , estimate (iii).

indeed are seen) but discrepancies are also apparent for other mobility ranges. The most complete expression for example introduces an error of about $10^{0.5}$ for the range of $\{10^{0.6}, 10^{0.7}\}$. Similar results were also seen for source A.

Application of the three estimates to source C produces Figure 11 for the magnitude and Figure 12 for the phase. As regards both components, the discrepancies introduced are greater than those seen for the mass-controlled sources.

2.2.1. *Discussion*

For both iterative and matrix inversion schemes applied to the estimation of the force ratios, discrepancies are seen, cf. the exact solution. Moreover, for all cases, the discrepancies were particularly large, where the point and transfer mobilities are of approximately equal magnitude. This is important, since for both mass- and

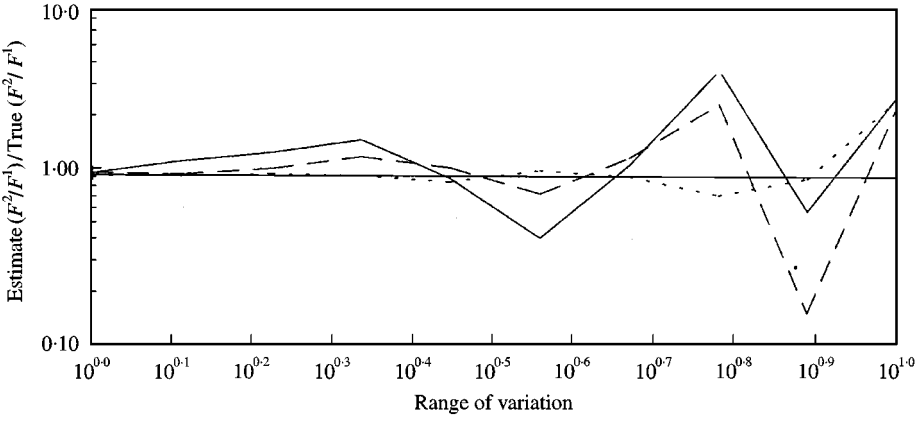

Figure 11. Truncation estimates for the magnitude of a resonance-controlled source. ——, Estimate (i); – – , estimate (ii); - - - - , estimate (iii).

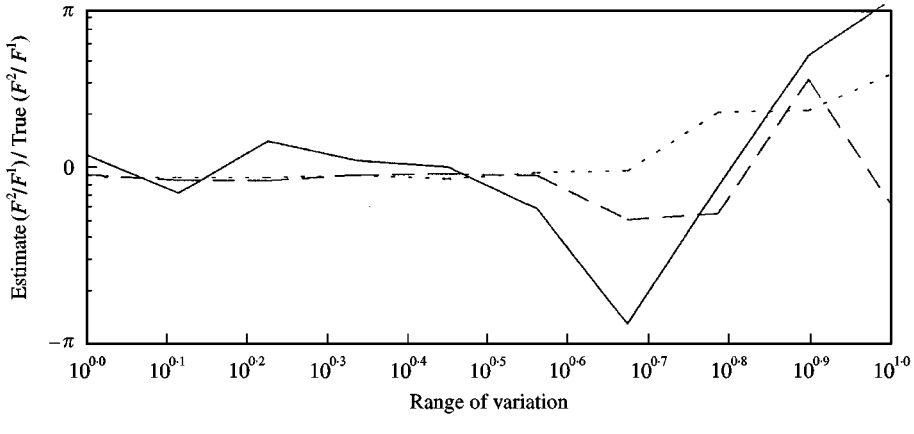

Figure 12. Truncation estimates for the phase of a resonance-controlled source. ——, Estimate (i); – – , estimate (ii); - - - - , estimate (iii).

resonant-controlled sources it is known that such mobility conditions are physically possible [3]. Unfortunately, it can be deduced therefore that for these source types none of the schemes considered will, in the practical situation, produce reliable estimates.

As regards a stiffness controlled source, though the phase of all the mobilities is $\pi/2$, the phase of the free velocities can assume a random value [3]. Via equation (13) the forces will therefore be complex, thus, it can be deduced that the results for the resonance-controlled source are also applicable for this source type. With a flange-like base, the magnitude of the transfer mobilities can be a decade below that of the point mobilities [3] to permit the suggestion that all three iterative methods would successfully estimate the force ratios after only 3 or 4 iterations. Moreover, with respect to the matrix inversion approach, even the simplest estimate would be likewise reliable. With a plate-like base, it is however known that the point and transfer mobilities can, as for a resonance-controlled source, approximate each other [3]. For these, both the iterative and matrix inversion schemes can therefore again be expected to be unreliable.

Physically, the success of the estimates for a stiffness-controlled source with a flange-like base is due to the points being uncoupled. For both mass- and resonance-controlled sources where this is not always so, the study reveals the force ratios to be sensitive to the transfer mobilities. This is important, for it suggests that to obtain the force ratios via a full inversion of the mobility matrix not only requires all the transfer mobilities but also accuracy of all these data. If the number of contact points and degrees of freedom is large and/or the frequency range of interest extended, the practical difficulties of obtaining such data are clear: i.e., consider the amount of spectra needed and the inherent problems of obtaining, via either measurement or prediction, accurately [8]. Further, it is also remembered that the above study only considers the constant force source case. Clearly, in the matched case where the force ratios are influenced by both source and receiver structures, the problems are compounded. This is especially significant with respect to maintaining the independence of the source descriptor.

Hence, it is inferred from the analytical study that the development of a methodology to estimate exactly the force ratios in a system is unlikely to ever be "fruitful". It is suggested therefore that a statistical approach towards estimating the force ratios be considered instead.

3. STATISTICAL STUDY

Invoking a statistical approach will inevitably incur a subsequent loss in the accuracy of the force ratio estimates and in any functions subsequently calculated from them: i.e., in the effective point mobilities, source descriptors, coupling functions and power. Whilst this is clearly unfortunate it can be somewhat alleviated if the statistical distribution of the functions are determined and confidence limits introduced. Provided that the range of, i.e. the 90% confidence limit, is small, the solution can be considered accurate to this small extent and henceforth of use. Before embarking upon the study it is important to note though

that, due to its cyclic nature, it is difficult to introduce confidence limits for the phase of the force ratios. This misfortune is very significant for without accurate phase information, a prediction of the possible maximum or minimum power transmitted cannot be made [2]: i.e., the relevance of the phase information with respect to the coupling function; see equation (2). With this in mind, an outcome of the study would therefore be to acknowledge the possibility of such extreme values but to find that they are statistically unlikely.

3.1. STATISTICAL DESCRIPTION OF SOURCE–RECEIVER SYSTEMS

Because the force ratios are influenced by a large number of parameters, i.e., all of the mobilities and all of the free velocities, a complete parametric study of their statistical properties is difficult. Hence, in order to "open the door" to an analysis, a simplified method for describing a system is proposed in which the number of independent parameters involved in greatly reduced.

The basis of the simplified description is to introduce the concept of grouped mobility functions. To realize these, the structural field, as described by a mobility matrix at a discrete frequency, is first considered as an Argand diagram; see Figure 13. Second, the mobility vectors are defined with respect to their individual magnitude and phase components and these then collated to form two populations; see Figure 14. Finally, the two populations are designated statistical distributions; see Figure 15. Together, these form the grouped mobility function.

Upon defining in a similar manner a grouped free velocity function, the considered multipoint-connected source-receiver system is then completely described by using only (i) the grouped source mobility function, (ii) the grouped receiver mobility function and (iii) the grouped free velocity function.

If the form of these distributions is known (or assumed) a description of the system is then achieved by using only six independent parameters, three defining a normalized value, i.e., the mean if the distribution is normal, and three defining the "spread", i.e., the standard deviation if the distribution is normal. Moreover, with regard to a specific study of the force ratios, these six independent parameters

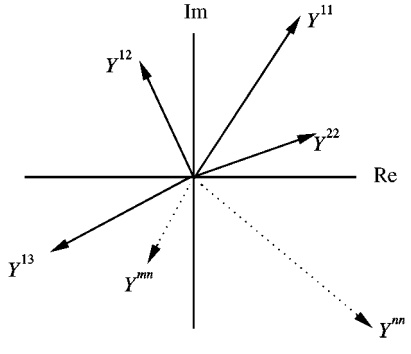

Figure 13. A mobility matrix represented using an Argand diagram format.

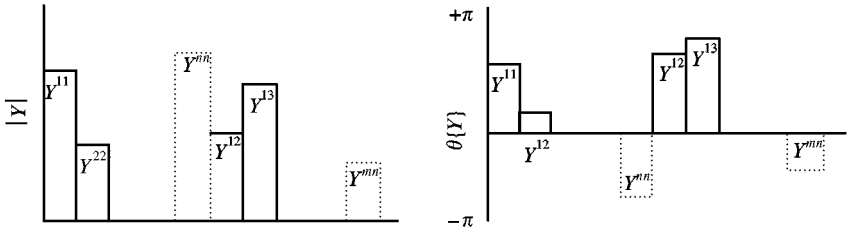

Figure 14. The mobility matrix represented as a population of (a) magnitudes and (b) phases.

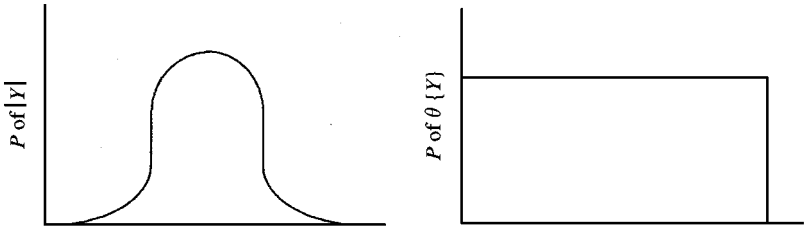

Figure 15. The populations of (a) the magnitudes and (b) the phases represented as statistical distributions.

can be further reduced to only four. To do so, a common denominator is introduced into equation (13) such that the normalized force can, essentially, be considered as a summation

$$F^n_{norm} = \frac{1}{Y_{common}} \sum_{t=1}^{24} \pm F^n_t, \tag{14}$$

where all the terms involved have the form

$$F^n_t = V^h_{sf}(Y^{ij}_s + Y^{ij}_r)(Y^{kl}_s + Y^{kl}_r)(Y^{mn}_s + Y^{mn}_r) \tag{15}$$

(all of h, i, j, k, l, m, n denote position) and the common denominator is

$$Y_{common} = (Y^{11}_s + Y^{11}_r)(Y^{22}_s + Y^{22}_r)(Y^{33}_s + Y^{33}_r)(Y^{44}_s + Y^{44}_r). \tag{16}$$

Upon taking the ratio of two forces the common denominator term cancels so that

$$F^m/F^n = F^m_{norm}/F^n_{norm} \Leftrightarrow \sum_{u=1}^{24} F^m_u \Big/ \sum_{t=1}^{24} F^n_t. \tag{17}$$

By concentrating then only on equation (15), this can be rewritten as

$$\begin{aligned} F^n_t = {} & (E[V^G_{sf}] + e\{V^h_{sf,t}\})(E[Y^G_s] + e\{Y^{ij}_{s,t}\} + E[Y^G_r] + e\{Y^{ij}_{r,t}\}) \\ & \times (E[Y^G_s] + e\{Y^{kl}_{s,t}\} + E[Y^G_r] + e\{Y^{kl}_{r,t}\}) \\ & \times E[Y^G_s] + e\{Y^{mn}_{s,t}\} + E[Y^G_r] + e\{Y^{mn}_{r,t}\}), \end{aligned} \tag{18}$$

so that if $e\{V_{sf}^h\}$ is divided by $E[V_{sf}^G]$ and the mobility terms are all divided by $E[Y_s^G]$ a normalized version can be produced:

$$F_{t,norm}^n = \left(1 + \frac{e\{V_{sf}^h\}}{E[V_{sf}^G]}\right)\left(1 + \frac{e\{Y_s^{ij}\}}{E[Y_s^G]} + \frac{E[Y_r^G]}{E[Y_s^G]} + \frac{e\{Y_r^{ij}\}}{E[Y_s^G]}\right)$$
$$\times\left(1 + \frac{e\{Y_s^{kl}\}}{E[Y_s^G]} + \frac{E[Y_r^G]}{E[Y_s^G]} + \frac{e\{Y_r^{kl}\}}{E[Y_s^G]}\right)\left(1 + \frac{e\{Y_s^{mn}\}}{E[Y_s^G]} + \frac{E[Y_r^G]}{E[Y_s^G]} + \frac{e\{Y_r^{mn}\}}{E[Y_s^G]}\right). \quad (19)$$

The number of independent parameters in use is thus seen to be only four: (i) $e\{V_{sf}^h\}$ normalized by $E[V_{sf}^G]$; (ii) $e\{Y_s^{ij}\}$ normalized by $E[Y_s^G]$; (iii) the ratio $E[Y_r^G]/E[Y_s^G]$; (iv) $e\{Y_r^{ij}\}$ normalized by $E[Y_s^G]$. Finally, to separate the source and receiver mobility conditions as much as possible the receiver mobility distribution can be renormalized by $E[Y_r^G]$ so that

$$\frac{e\{Y_r^{ij}\}}{E[Y_r^G]} = \frac{e\{Y_r^{ij}\}}{E[Y_s^G]} \Big/ \frac{E[Y_r^G]}{E[Y_s^G]}. \quad (20)$$

Prior to continuing the present study, it can be noted that the grouped function approach is not restricted to only one directional component and the "moment problem" can be incorporated. Were rotational motion also included in the model for example, then a further grouped "moment" mobility function could be introduced to take into account such a coupling. An associated grouped "rotational" free velocity function then, clearly, also is needed. A feature of introducing other directional components would then be to increase the number of independent parameters in the model. It is hoped that the relevance of this would be studied and supported in a forthcoming paper.

3.2. STATISTICAL DISTRIBUTIONS OF THE GROUPED MOBILITY FUNCTIONS

Beginning with the mobility phase, the distributions which define the grouped functions are now considered. The distributions are determined with respect to each of a structure characteristic mass, stiffness, resonant-controlled and infinite regions for which results from the authors' earlier paper [3] has been utilized.

Though it has already been shown that for a stiffness controlled, constant force source with a flange-like base the forces can (due to the contact points being uncoupled) be obtained via an analytical approach, this system type is included in the study in order to establish the statistical likelihood of such uncoupling (with flange number). Moreover, it is also retained so that it can be studied within the situation of mobility matched source and receivers.

Depending upon inertial properties, the phases of the mobilities of a mass-controlled source are discretized at either $\pm\pi/2$. Also deterministic is the phase of the mobilities of a stiffness-controlled source which for both point and transfer mobilities is $\pi/2$. Hence, in both cases, the distribution of the mobility phase does not have to be considered. For a resonance-controlled source the mobility phase can however assume any value between $\pm\pi$ and within the grouped mobility concept has to be therefore be defined. For want of further

studies, a uniform distribution is, as assumed in Statistical Energy Analysis [8], suggested.

For an insight into the distribution of the mobility magnitude, the general modal expansion formulation for the mobility of a distributed structure is considered,

$$Y(x, x_0) = \frac{\mathrm{i}\omega}{m} \sum_{n=1}^{N} \frac{\psi_n(x_0)\psi_n(x)}{\omega_n^2 - \omega^2 - \mathrm{i}\omega_n\omega\eta} \tag{21}$$

where the ratio Y^{ij}/Y^{kl} is obtained as

$$Y^{ij}/Y^{kl} = \sum_{n=1}^{N} \psi_n(x)/\psi_n(x_0), \tag{22}$$

to reveal that in a resonance region the distribution of the mobility magnitude can be obtained only if all the eigenfunctions are known. This provides a dilemma since, on the one hand, these cannot be determined without an exact definition of the structure while, on the other, a purpose of the grouped mobility concept is to avoid having an exact definition of the structure.

To help circumvent the dilemma, an assumption is introduced whereby the eigenfunctions of a "general" structure in a resonance controlled region are "said to be" sinusoidal with unit magnitude and random phase. By invoking this and, assuming too[†] that the modal summation can be truncated at $N = 5$, permits creation of "general" point and transfer mobilities. From a population of such mobilities a "general" distribution of the magnitude can then be obtained. The process is illustrated in Figure 16.

For a total population of 1000, the cumulative probability distribution function PDF [10] of $\log 10(|Y^{mn}/Y^{nn}|)$ is shown Figure 17. (A total of 1000 only was chosen so as to generate a statistically "reliable" population.) Also shown in the corresponding function for an "exact" log 10 normal distribution as calculated by using the mean and standard deviation of the population. Thus, because of the closeness of the two results, it is suggested that the grouped mobilities of a resonance-controlled source have a log 10 normal[‡] magnitude distribution.

For a mass-controlled source, the mobility ratio is given by

$$\frac{Y^{ij}}{Y^{kl}} = \frac{(k_{yy}^2 + y_0 y(k_{yy}^2/k_{xx}^2) - x_0 x)}{(k_{yy}^2 + y_0^2(k_{yy}^2/k_{xx}^2) - x_0^2)}, \tag{23}$$

and this is seen to be dependent upon the positions of the contact points, the ratio of the two radii of gyration along with the value of one of the radii of gyration (k_{yy}^2 in this case although if the expression had been normalized by using k_{yy}^2, then k_{xx}^2 would be the dependent parameter). Likewise for a resonance-controlled source

[†]From SEA it is known that if the number of modes included in the sum is at least 5 then the phase of the mobility can be considered random with a uniform distribution. With five modes, the distribution of the phase is therefore in agreement with that assumed for the mobility phase in a resonant region.

[‡]It can be noted that in traditional statistics a lognormal distribution is given to base e [10]. Because in this study the mobility data is transformed using log 10 the term log 10normal is used. The only difference between the two definitions is in the value of the standard deviation.

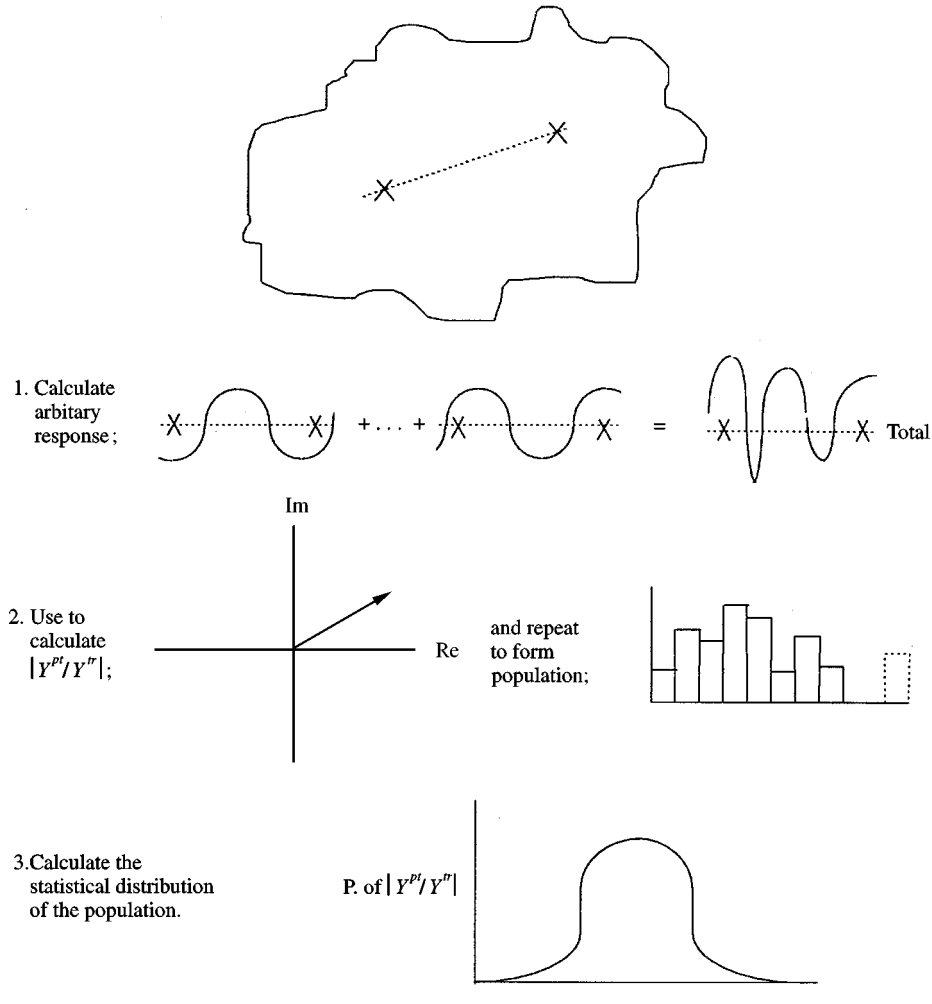

Figure 16. Generating the statistical distribution of a 'general' grouped mobility function for a resonance-controlled source.

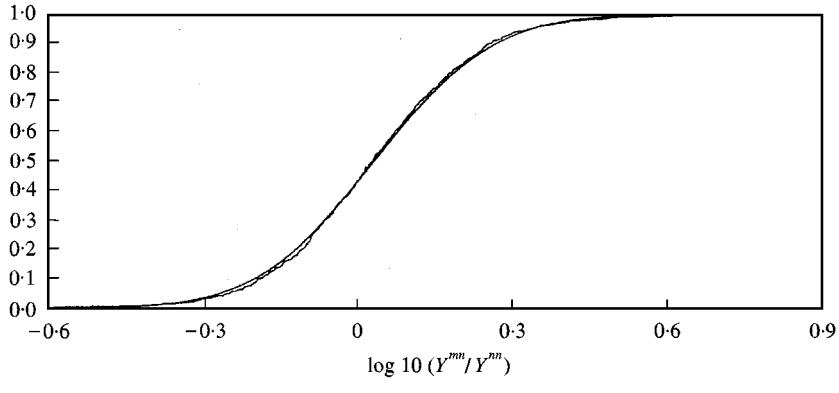

Figure 17. PDF for resonance-controlled source.

the inherent dilemma is therefore that without an exact definition of the system the mobility distribution cannot be determined but that such information is converse to the grouped mobility concept. Again, therefore, an assumption has to be made.

As a "stab in the dark", and therefore without recourse to a further study, it is simply suggested that for a mass-controlled source the magnitude of the grouped mobilities has, and likewise the resonance-controlled source, a log 10 normal distribution. For a symmetric, as opposed to a non-symmetric mass-controlled source, a distinction can be made where the mobilities are paired in accordance with the machine's symmetrical properties. This is illustrated in Figures 18 and 19.

Upon consideration of a stiffness-controlled source, it is realized that Y^{mn}/Y^{nn} is dependent upon the mount size, the type of mounting (plate- or flange-like), the position of the contact points and the boundary conditions of the mounts [3]. The dilemma encountered with the resonance and mass-controlled sources is therefore apparent and hence it is necessary to introduce an assumed distribution for the grouped mobility magnitude. Again without reference to a further study, but to keep the descriptions consistent, it is suggested that when the base is plate-like, a log 10 normal distribution be adopted, and likewise for a mass-controlled source, although a distinction can be made between symmetric and non-symmetric structures.

For a flange-like base, the important phenomena, owing to which the magnitude of the transfer mobility is an order of magnitude less than that of the point mobility,

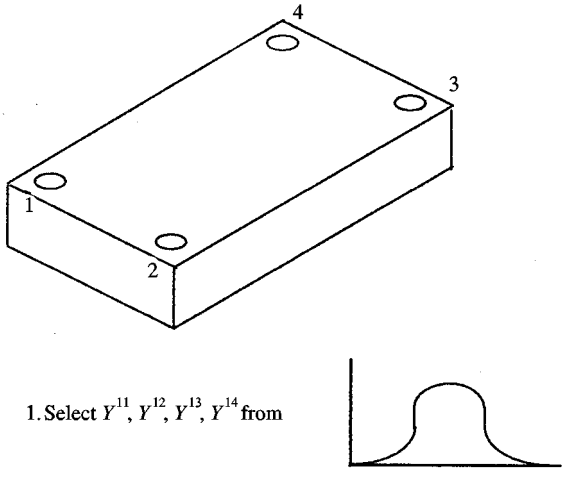

Figure 18. Obtaining from the grouped mobility function, the mobility matrix for a mass-controlled source with symmetric geometry.

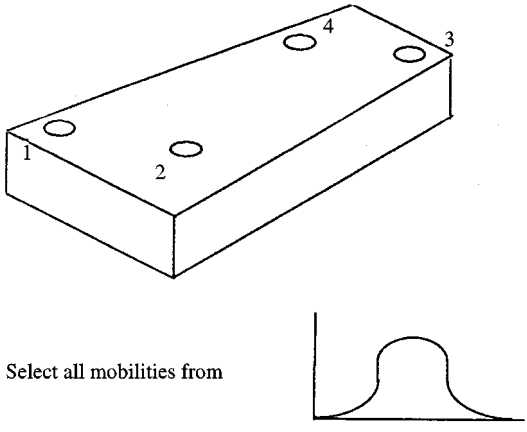

Figure 19. Obtaining from the grouped mobility function, the mobility matrix for a mass-controlled source with non-symmetric geometry.

can be incorporated into the grouped mobility concept by assuming a log 10normal distribution only for the point mobilities and with the introduction of

$$Y^{mn} = \frac{(Y^{mm} + Y^{nn})}{2} \Big/ 10. \tag{24}$$

Similarly, for a strong discontinuity for which the tranfer mobility is negligible

$$Y^{mn} = 0 \tag{25}$$

can be introduced. These ideas are illustrated in Figure 20.

With respect to the receiver, similar properties are suggested for its grouped mobility distributions. Hence, for a stiffness-controlled receiver the phase is considered deterministic at $\pi/2$ and the magnitude assumed to form a log 10 normal distribution. Likewise, for a resonance-controlled receiver a log 10 normal distribution is assumed for the magnitude of the mobilities and a uniform distribution for the phase.

In addition to these two cases, an infinite region can also exist for the receiver where, if all contact points are separated by distances greater than one-eighth of a wavelength, the magnitude of Y^{mn}/Y^{nn} is (increasingly) distance-dependent and therefore undeterministic. To be consistent with the rest of the study, the distribution is also suggested to be log 10 normal in this situation. Regarding the phase, while in the infinite region this is deterministic at $\pi/2$ for the point mobilities, it is undeterministic for the transfer mobilities, where a uniform distribution is suggested. As for both the mass- and stiffness-controlled sources, the semi-deterministic nature of the region means the mobilities can, if symmetric geometry is assumed, be paired.

Thus upon assuming a log 10 normal distribution for the magnitude of the grouped mobility function, typical values for the standard deviation need to be considered. So to coerce the study, physically realistic values need to be imposed.

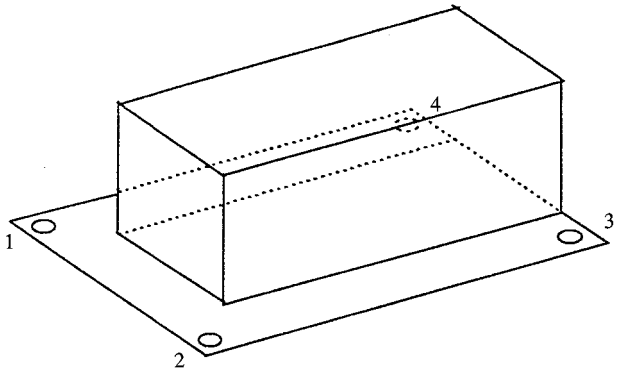

1. Select Y^{11}, Y^{13} *and* Y^{44} from

2. $Y^{11} = Y^{22}$

$Y^{33} = Y^{44}$

$Y^{12} = ((Y^{11} + Y^{22})/2)/10$

$Y^{23} = Y^{14} = ((Y^{11} + Y^{44})/2)/10$

$Y^{34} = 0$

$Y^{13} = Y^{24}$

Figure 20. obtaining from the grouped mobility function, the mobility matrix for a 3-flange stiffness controlled source with non-symmetric geometry.

To obtain a practical lower limit, it is recognized that the condition can exist where all the mobility magnitudes are equal, or are very nearly so. This can occur, for example, at the fundamental resonance of a plate-like structure. In this situation, the standard deviation of the mobilities is clearly small and can, approach zero, and this was therefore imposed as a lower limit.

For an insight towards obtaining a practical value for the upper limit a normalized standard deviation was extracted from a number of experimental case studies by using the ratio,

$$\varepsilon_Y = \log 10 (\max\{Y^G\}/\min\{Y^G\}), \tag{26}$$

and assuming this to represent four standard deviations. A typical result based upon the mobility data of an industrial fan unit [3] is shown in Figure 21. In all cases studied ε_Y was never found to exceed 4 (i.e., $Y^{\max}/Y^{\min} < 10^4$), so an upper limit of $\log 10(10^1) = 1$ was adopted. To rationalize the study, the same limits were assumed regardless of the structural controlling mechanism (mass, stiffness, etc.)†.

†Refinement of the conditions can be considered as part of a further study, i.e., the mobilities for a finite plate are more likely to have a high standard deviation than for an infinite plate where mobility differences occur only because of divergence.

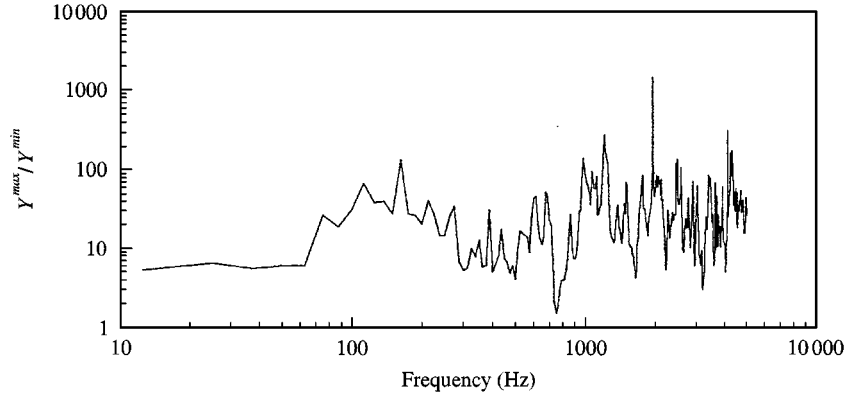

Figure 21. Y^{max}/Y^{min} for typical fan unit.

Finally, to complete the statistical description of the mobilities, the ratio of $\log 10(E[Y_r^G]/E[Y_s^G])$ had to be considered. Based upon an assumption that the magnitude of the receiver mobility never exceeds that of the source, an upper limit of $\log 10(1) = 0$ was introduced. A lower limit was determined based upon the assertion that for the study to be thorough it should be such that the constant force situation is attained. This, it was suggested, can be ensured by using a lower limit of 10^{-5}: i.e., as $\log 10(10^{-5}) = -5$, the mean of the receiver mobilities is 100 dB less than that of the source mobilities.

The source conditions are summarized in Table 1 and the receiver conditions in Table 2.

3.3. STATISTICAL DISTRIBUTION OF THE FREE VELOCITIES

To complete the description of the system the grouped free velocity function is needed. A clear difficulty here is that the free velocities depend upon the many different excitation mechanisms of the source. Where, for a general insight, nothing about this is defined, it is difficult to conceive of a study through which anything at all about them can be determined. Even, for example, a general formulation comparable to the modal expansion utilized for the mobilities, i.e., equation (21), cannot be suggested. Upon consideration of this misfortune, but with determination to forward the study, it is therefore, most simply suggested that the magnitude of the grouped free velocity function be considered to have, for the grouped mobility function, a log 10 normal distribution for all source types. As regards the phase, this can be considered as being discretized at either 0 or π for a mass-controlled source or, to have a uniform distribution for both a resonance- and stiffness-controlled source.

Suitable practical values for the standard deviation of the magnitude distribution were, likewise for the mobilities, obtained from measured data. From an industrial fan unit, Figure 22 is a typical result for ε_V. For all cases studied, ε_V was found to be between 10^0 and 10^4 where a range of 0–1 was again adopted.

The free velocity conditions are summarized in Table 3.

TABLE 1

Set-up conditions for source mobility

Description	Source mobility												
	Mass controlled				Stiffness controlled								
	Symmetric		Non-symmetric		Symmetric				Non-symmetric				
	High I_{xx} Low I_{yy}	Low I_{xx} High I_{yy}	High I_{xx} Low I_{yy}	Low I_{xx} High I_{yy}	Plate	2-flange	3-flange	4-flange	2-flange	3-flange	4-flange	Plate	Resonance controlled
Magnitude	$\{Y_{11}, Y_{12}, Y_{13}, Y_{14}\}$ = log 10normal PDF $Y_{11} = Y_{22} = Y_{33} = Y_{44}$ $Y_{12} = Y_{34}$ $Y_{13} = Y_{24}$ $Y_{14} = Y_{23}$ ①		$\{Y_{mn}\}$ = log 10normal PDF ②		As ①	$\{Y_{11}, Y_{44}\}$ = log 10normal PDF $Y_{11} = Y_{22}, Y_{33} = Y_{44}$ $Y_{14} = Y_{23} = (Y_{11} + Y_{44})/20$ $Y_{12} = Y_{34} = Y_{13} = Y_{24} = 0$	$Y_{11} = Y_{22}, Y_{33} = Y_{44}$ $Y_{14} = Y_{23} = (Y_{11} + Y_{44})/20$ $Y_{34} = Y_{13} = Y_{24} = 0$ $Y_{12} = (Y_{11} + Y_{22})/20$	$Y_{11} = Y_{22}, Y_{33} = Y_{44}$ $Y_{14} = Y_{23} = (Y_{11} + Y_{44})/20$ $Y_{13} = Y_{24} = 0$ $Y_{12} = Y_{34} = (Y_{11} + Y_{22})/20$	$\{Y_{pt}\}$ = log 10normal PDF $Y_{12} = Y_{34} = Y_{13} = Y_{24} = 0$ $Y_{14} = Y_{23} = (Y_{11} + Y_{44})/20$ $Y_{23} = (Y_{22} + Y_{33})/20$	$Y_{12} = (Y_{11} + Y_{22})/20$ $Y_{13} = Y_{24} = 0$ $Y_{14} = (Y_{11} + Y_{44})/20$ $Y_{23} = (Y_{22} + Y_{33})/20$	$Y_{12} = (Y_{11} + Y_{22})/20$ $Y_{13} = Y_{24} = 0$ $Y_{14} = (Y_{11} + Y_{44})/20$ $Y_{23} = (Y_{22} + Y_{33})/20$ $Y_{34} = (Y_{33} + Y_{44})/20$	As ②	
Phase	$\theta\{Y_{14}\} = \theta\{Y_{11}\} = \pi/2$ $\theta\{Y_{12}\} = \theta\{Y_{13}\} = \pi/2$	$\theta\{Y_{12}\} = \theta\{Y_{11}\} = \pi/2$ $\theta\{Y_{13}\} = \theta\{Y_{14}\} = \pi/2$	$\theta\{Y_{14}\} = \theta\{Y_{11}\} = \pi/2$ $\theta\{Y_{12}\} = \theta\{Y_{13}\} = \pi/2$	$\theta\{Y_{12}\} = \theta\{Y_{11}\} = \pi/2$ $\theta\{Y_{13}\} = \theta\{Y_{14}\} = \pi/2$		$\theta\{Y^{mn}\} = \pi/2$						$\theta\{Y^{mn}\}$ = random	

TABLE 2

Set-up conditions for receiver mobility

	Receiver mobility				
	Stiffness controlled plate		Resonance-controlled		
				Infinite plate region	
Description	Symmetric	Non-symmetric	Finite plate	Non-symmetric	Symmetric
Magnitude	As ①		As ②		As ①
Phase	$\theta\{Y^{mn}\} = \pi/2$		$\theta\{Y_{mn}\} =$ random	$\theta\{Y^{pt}\} = 0$ $\theta\{Y^{tr}\} =$ random	

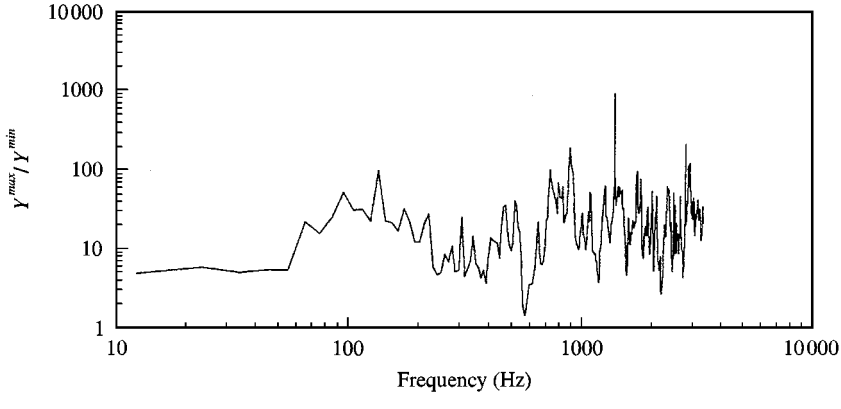

Figure 22. V^{max}/V^{min} for typical fan unit.

3.4. DISTRIBUTION OF THE FORCE RATIOS

A methodology through which the suggested grouped functions can be used to study the statistical distribution of the force ratios is now considered. While conceptually this could be based upon mathematical "meanderings" around the expression for the force ratios, it is suggested that this would be rather difficult and the development obtuse. The expression for the force ratios does after all involve the ratio of two summations,

$$F^m/F^n = \sum_{u=1}^{24} F_u^m \Big/ \sum_{l=1}^{24} F_t^n, \tag{27}$$

where each term in the summations has the form

$$\{F_t\} = (\{V_{sf,t}^h\})(\{Y_{s,t}^{ij}\} + \{Y_{r,t}^{ij}\})(\{Y_{s,t}^{kl}\} + \{Y_{r,t}^{kl}\})(\{Y_{s,t}^{mn}\} + \{Y_{r,t}^{mn}\}), \tag{28}$$

TABLE 3

Set-up conditions for free velocity

	FREE VELOCITY				
		Mass controlled			
Description	Vertical motion	X-axis rotation	Y-axis rotation	Stiffness controlled	Resonance controlled
Magnitude	$\{V_{sf}^1, V_{sf}^2, V_{sf}^3, V_{sf}^4\} = \log 10\text{normal PDF}$				
Phase	$\theta\{V_{sf}^N\} = 0$	$\theta\{V_{sf}^1\} = 0$ $\theta\{V_{sf}^2\} = 0$ $\theta\{V_{sf}^3\} = \pi$ $\theta\{V_{sf}^4\} = \pi$	$\theta\{V_{sf}^1\} = 0$ $\theta\{V_{sf}^4\} = 0$ $\theta\{V_{sf}^2\} = \pi$ $\theta\{V_{sf}^3\} = \pi$	$\theta\{V_{sf}^N\} = \text{random}$	

such that, to the authors, it is not obvious along what path a mathematical study would follow. Therefore, a methodology based upon a Monte Carlo sampling method [12] was developed.

Firstly, magnitudes and phases for mobilities and free velocities were randomly selected from the appropriate grouped functions. These were then used to form a fictive system for which, by using equation (4), the force ratios were calculated. The procedure was repeated N times to form a population of force ratios and, of this, the statistical distribution was assessed. The methodology is illustrated in Figure 23 for the case of a resonance-controlled source attached to a resonance-controlled receiver.

For a sample population of 1000, the PDF of $|(F^2/F^1)|$ is shown in Figure 24 for a "typical" resonance-controlled source described by using a grouped mobility function with a magnitude standard deviation of $10^{0{\cdot}4}$ and a grouped free velocity function with a magnitude standard deviation of $10^{0{\cdot}2}$. For the same magnitude conditions but, as appropriate, different phase relationships, the PDF of $|(F^2/F^1)|$ for a non-symmetric mass-controlled source is also shown (see Figure 25). An equivalent log 10 normal PDF as calculated by using the mean and standard deviation of the populations supplements both figures. Comparing the true and equivalent PDFs reveals close agreement. (This, it is suggested, is a consequence of the central limit theorem [10].) That such unison was also seen for other source conditions establishes that the distribution of the force ratio magnitude can be assumed log 10 normal. With such an assumption, the resultant PDF of a force ratio can then be defined upon knowing only the mean and the standard deviation.

As regards the phase of the force ratios, it can be deduced that for those source conditions where either the phase of the grouped free velocity function or of the grouped mobility function is random, it also will be random. Regardless of the source–receiver mobility matching condition and of the receiver controlling mechanism, this will therefore, because of the nature of the grouped free velocity function at least, be so when the source is either stiffness or resonance controlled.

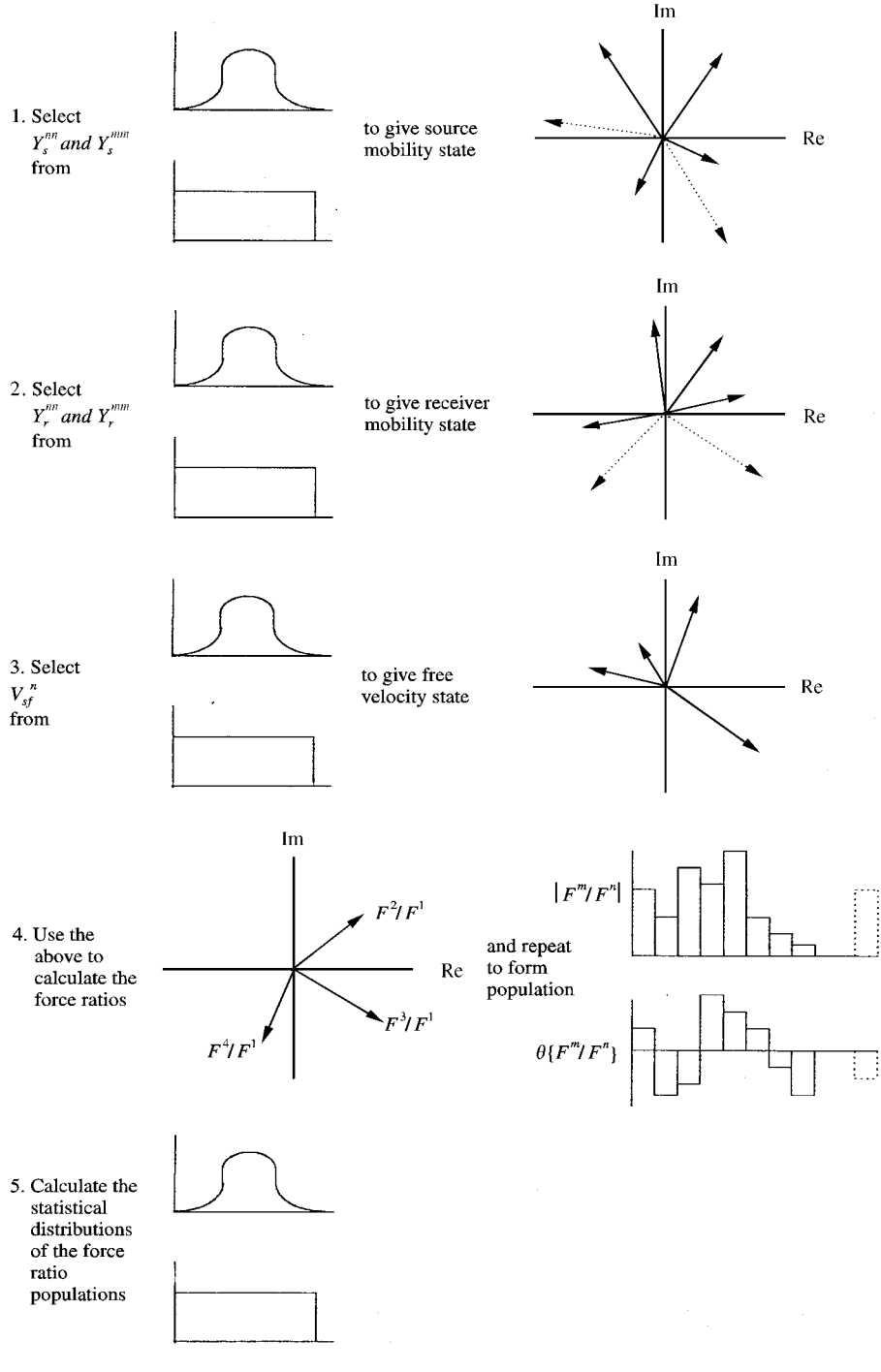

Figure 23. For a resonance-controlled source matched to a resonance-controlled receiver, the methodology implemented to obtain the statistical distribution of the force ratios.

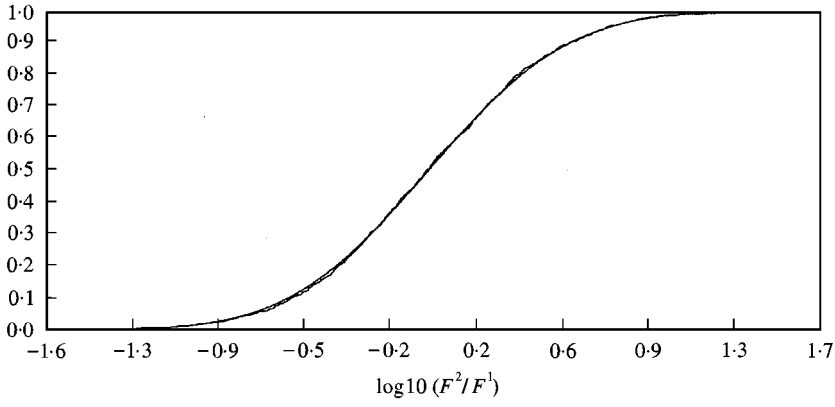

Figure 24. PDF of F^2/F^1 for resonance-controlled source.

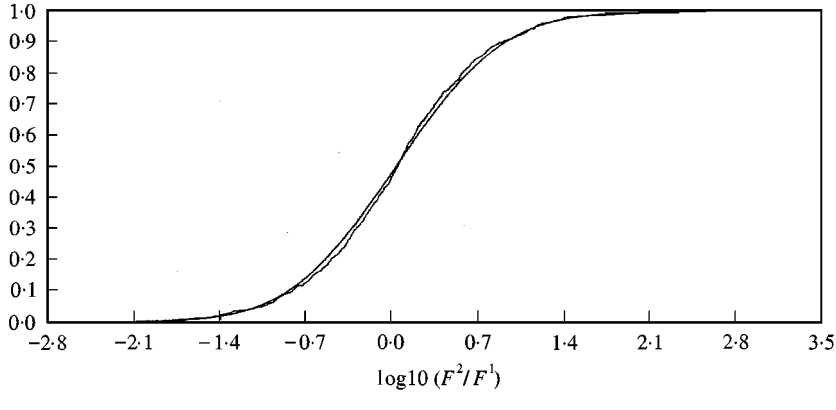

Figure 25. PDF of F^2/F^1 for mass-controlled source, high I_{xx}, low I_{yy}, rotational excitation about the x-axis ——, Calculated; - - - - - , equivalent.

For a mass-controlled source, a random condition will be apparent only when it is attached to a resonance-controlled receiver and when both structures' are mobility matched. For all other cases involving a mass-controlled source the force ratios will have a phase which is discretized at either 0 or $\pm\pi$ but which of these cannot be assessed. This is so since the forces as given by equation (4) have the form

$$F^n_{norm} = \sum_{t=1}^{24} \pm \mathrm{Re}\{V^h_{sf,t}\}\,\mathrm{Im}\{Y^{ij}_{s,t}\}\,\mathrm{Im}\{Y^{kl}_{s,t}\}\,\mathrm{Im}\{Y^{mn}_{s,t}\}, \tag{29}$$

which is essentially a summation of $\pm$ terms of random magnitude. In the study, therefore, one can consider only the magnitude of the force ratio distribution.

3.5. FORCE RATIO MAGNITUDE DISTRIBUTION FOR A CONSTANT FORCE SOURCE

Whilst for a mass-controlled source four different grouped mobility functions and three different grouped free velocity functions have been defined there is, with

regards to the resultant system description, some redundancy. A source with high I_{xx}, low I_{yy} rotated around the x-axis for example is equivalent to a source with low I_{xx}, high I_{yy} rotated around the y-axis. When all such redundancies are omitted, six distinct mass-controlled CFS systems remain. In relation to a stiffness or resonance-controlled source, the number of distinct conditions is, by nature of their having only one free velocity condition, simply the number of different grouped mobility functions proposed: i.e., eight for a stiffness-controlled source and one for a resonance-controlled source.

Upon implementation of the methodology, the size of the sampled population was, due to the number of different situations considered and the limiting speed of the CPU, limited to 2000. Also due to time constraints, the standard deviation of the grouped functions were considered only in increments of 0·2.

A selection representative of the forthcoming results are presented.

3.5.1. *Mass-controlled source*

For a source that is symmetric and mass controlled with high I_{yy}, low I_{xx} and undergoing translational excitation (see Figure 1), the resultant standard deviation (upper family of curves) and mean (lower family of curves) of log 10 $|(F^2/F^1)|$ and $|(F^4/F^1)|$ are shown in Figure 26. The x-axis is the standard deviation of the normalized source mobilities and each line type on the figure represents a different $\sigma\{V_{sf}^G\}$. For the same source type but with non-symmetric geometry imposed (likewise Figure 19) the corresponding results are shown in Figure 27.

For both cases it is suggested that the mean of the force ratios is independent of (or insensitive to) both $\sigma\{V_{sf}^G\}$ and $\sigma\{Y_s^G\}$ and simply tends to $10^0 = 1$. As regards the standard deviation, the suggestion is however that for a symmetric source it has a dependency upon both $\sigma\{V_{sf}^G\}$ and $\sigma\{Y_s^G\}$ while for a non-symmetric source the dependency is only upon $\sigma\{Y_s^G\}$. Although for the symmetric case it is difficult to determine the inter-relationship between the variables, for the non-symmetric case a linear relationship can be proposed. Moreover, for this case a unison between $|(F^2/F^1)|$ and $|(F^4/F^1)|$[†] is suggested such that the same relationship applies to both.

Hence, by using the method of least squares [10] a resulting empirical equation for $\sigma\{(F^m/F^n)\}$ for a non-symmetric mass-controlled source with high I_{yy} and low I_{xx} undergoing translational excitation can be suggested,

$$\sigma\{(F^m/F^n)\} \approx 0{\cdot}5 \times \sigma\{Y_s^G\} + 0{\cdot}5, \tag{30}$$

where each standard deviation characterizes a log 10 normal distribution.

For $\sigma\{Y_s^G\} = 0{\cdot}2$, equation (30) gives $\sigma\{(F^m/F^n)\} = 0{\cdot}6$ whilst for $\sigma\{Y_s^G\} = 1$, it gives $\sigma\{(F^m/F^n)\} = 1$. These are larger than the comparable values for the symmetric case so that it can be said that the uncertainty of (F^m/F^n) increases for non-symmetrical, cf. symmetrical geometry. This can be expected since the number of independent mobilities for the non-symmetrical case is 10 compared to just 4 for the symmetric case.

[†]Throughout the remainder of the paper the magnitude bars are ignored and the notation (F^m/F^n) used to done the magnitude of a general force ratio for which no specific points are named.

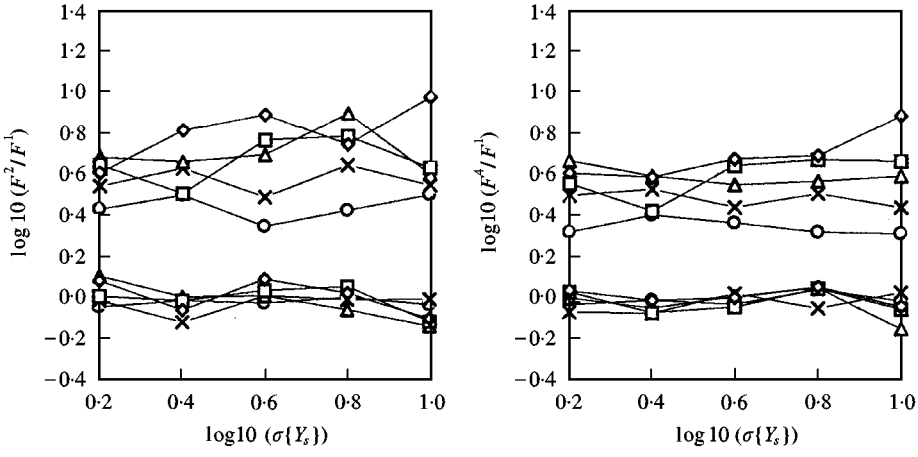

Figure 26. Force ratio statistics for symmetric mass-controlled source, high I_{yy}, low I_{xx}, translational excitation. The x-axis represents the standard deviation of the grouped source mobilities. Their distribution is assumed to be log 10normal. The y-axis represents the distribution of the force ratios whereby the lower family of curves is the mean and the upper family of curves is the standard deviation. Again the distribution is assumed log 10normal. Each line on the figures is a different standard deviation of a free velocity log 10normal distribution: –◇– $\sigma\{V_{sf}^G\} = 1{\cdot}0$; –□–, $\sigma\{V_{sf}^G\} = 0{\cdot}8$; –△–, $\sigma\{V_{sf}^G\} = 0{\cdot}6$; – × –, $\sigma\{V_{sf}^G\} = 0{\cdot}4$; –○–, $\sigma\{V_{sf}^G\} = 0{\cdot}2$.

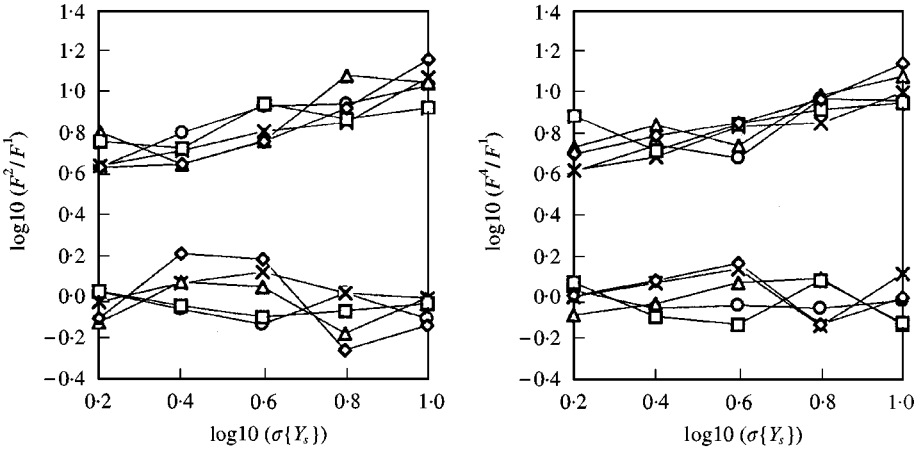

Figure 27. Force ratio statistics for non-symmetric mass-controlled source, high I_{yy}, low I_{xx}, translational excitation. The x-axis represents the standard deviation of the grouped source mobilities. Their distribution is assumed to be log 10normal. The y-axis represents the distribution of the force ratios whereby the lower family of curves is the mean and the upper family of curves is the standard deviation. Again the distribution is assumed log 10normal. Each line on the figures is a different standard deviation of a free velocity log 10normal distribution: –◇– $\sigma\{V_{sf}^G\} = 1{\cdot}0$; –□–, $\sigma\{V_{sf}^G\} = 0{\cdot}8$; –△–, $\sigma\{V_{sf}^G\} = 0{\cdot}6$; – × –, $\sigma\{V_{sf}^G\} = 0{\cdot}4$; –○–, $\sigma\{V_{sf}^G\} = 0{\cdot}2$.

For the same source but with rotational excitation about the y-axis, i.e., rotation about a low inertia axis (see Figure 2), $\sigma\{(F^2/F^1)\}$ is shown in Figure 28 for an imposed symmetric geometry. Upon comparison with the case of translational excitation (Figure 26) the statistics are suggested to be similar. Such unison was also

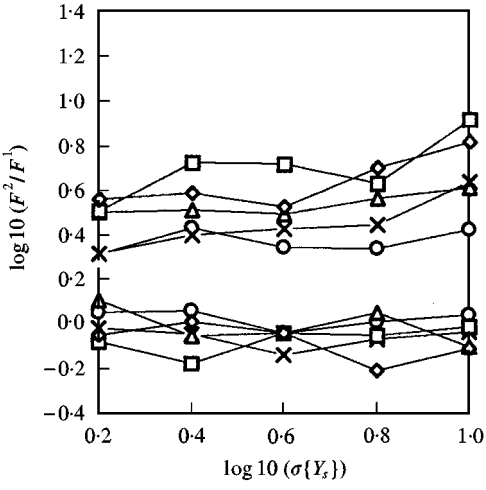

Figure 28. Force ratio statistics for symmetric mass-controlled source, high I_{yy}, low I_{xx}, rotational excitation about the y-axis. The x-axis represents the standard deviation of the grouped source mobilities. Their distribution is assumed to be log 10normal. The y-axis represents the distribution of the force ratios whereby the lower family of curves is the mean and the upper family of curves is the standard deviation. Again the distribution is assumed log 10normal. Each line on the figures is a different standard deviation of a free velocity log 10normal distribution: $-\diamond-$ $\sigma\{V_{sf}^G\} = 1{\cdot}0$; $-\square-$, $\sigma\{V_{sf}^G\} = 0{\cdot}8$; $-\triangle-$, $\sigma\{V_{sf}^G\} = 0{\cdot}6$; $-\times-$, $\sigma\{V_{sf}^G\} = 0{\cdot}4$; $-\bigcirc-$, $\sigma\{V_{sf}^G\} = 0{\cdot}2$.

seen for the other force ratios and also when a non-symmetric condition was imposed. Moreover, with rotational excitation about the x-axis, i.e., rotation about a high inertia axis, the resultant force ratio statistics were also found to be similar. This means that with respect to the force ratio statistics, the distinct CFS systems are not distinguishable and equation (30) applies for all systems with a non-symmetric condition.

3.5.2. *Stiffness-controlled source*

For a stiffness-controlled source with a plate-like base (see Figure 29), the mean and standard deviation of (F^2/F^1) are shown for symmetrical geometry in Figure 30 and for non-symmetrical geometry in Figure 31. Likewise for the mass-controlled source the standard deviation is dependent upon both $\sigma\{V_{sf}^G\}$ and $\sigma\{Y_s^G\}$ for symmetric geometry but only upon $\sigma\{Y_s^G\}$ for non-symmetric geometry. Also likewise the mass-controlled source, the mean is independent of both $\sigma\{V_{sf}^G\}$ and $\sigma\{Y_s^G\}$ and tends to unity. Similar results were seen for the other force ratios.

Fitting a linear regression line to the standard deviation of the non-symmetrical geometry gives the relationship between $\sigma\{(F^m/F^n)\}$ and $\sigma\{Y_s^G\}$ as

$$\sigma\{(F^m/F^n)\} \approx 0{\cdot}7 \times \sigma\{Y_s^G\} + 0{\cdot}3, \tag{31}$$

where, compared to the non-symmetric mass-controlled source, a slight decrease in the uncertainty of $\sigma\{(F^m/F^n)\}$ for low values of $\sigma\{Y_s^G\}$ is revealed.

The statistics of (F^2/F^1) resultant for a stiffness-controlled source with a 2-flange-like base (see Figure 32) are shown in Figure 33 for an imposed

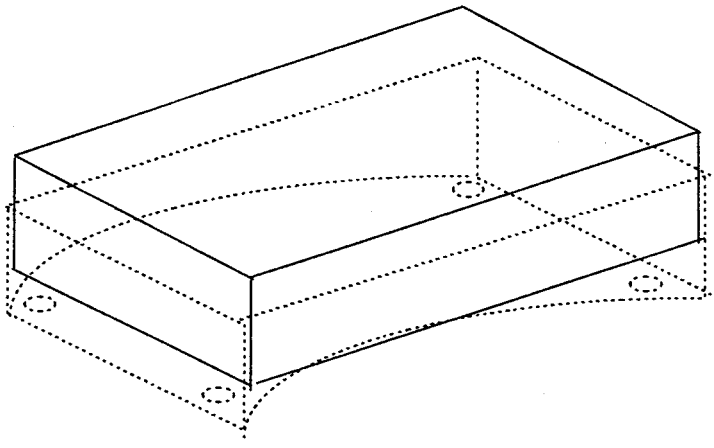

Figure 29. A source with a plate-like base with stiffness-controlled behaviour.

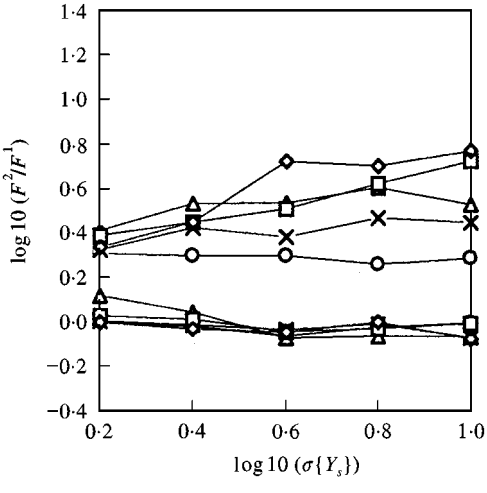

Figure 30. Force ratio statistics for symmetric stiffness-controlled source with a plate-like base. The x-axis represents the standard deviation of the grouped source mobilities. Their distribution is assumed to be log 10normal. The y-axis represents the distribution of the force ratios whereby the lower family of curves is the mean and the upper family of curves is the standard deviation. Again the distribution is assumed log 10normal. Each line on the figures is a different standard deviation of a free velocity log 10normal distribution: –◇– $\sigma\{V_{sf}^G\} = 1{\cdot}0$; –□–, $\sigma\{V_{sf}^G\} = 0{\cdot}8$; –△–, $\sigma\{V_{sf}^G\} = 0{\cdot}6$; – × –, $\sigma\{V_{sf}^G\} = 0{\cdot}4$; –○–, $\sigma\{V_{sf}^G\} = 0{\cdot}2$.

symmetric geometry and in Figure 34 for non-symmetric geometry. Once again it is suggested that as regards the standard deviation this depends only upon $\sigma\{Y_s^G\}$ for non-symmetric geometry but upon both $\sigma\{V_{sf}^G\}$ and $\sigma\{Y_s^G\}$ for symmetric geometry. As regards the mean, this is, also as before, simply unity for all conditions. While the results for both $\sigma\{(F^3/F^1)\}$ and $\sigma\{(F^4/F^1)\}$ were found to differ from those of $\sigma\{(F^2/F^1)\}$ this can be considered unimportant since their influence is between points where a strong discontinuity has been assumed, i.e., both Y^{13} and Y^{14} have been defined as 0.

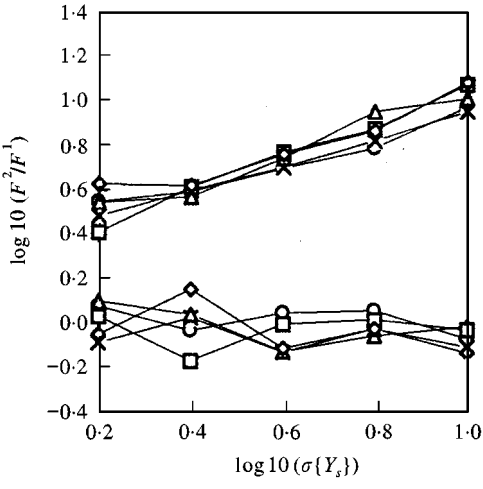

Figure 31. Force ratio statistics for non-symmetric stiffness-controlled source with a plate-like base. The x-axis represents the standard deviation of the grouped source mobilities. Their distribution is assumed to be log 10normal. The y-axis represents the distribution of the force ratios whereby the lower family of curves is the mean and the upper family of curves is the standard deviation. Again the distribution is assumed log 10normal. Each line on the figures is a different standard deviation of a free velocity log 10normal distribution: –◇– $\sigma\{V_{sf}^G\} = 1{\cdot}0$; –□–, $\sigma\{V_{sf}^G\} = 0{\cdot}8$; –△–, $\sigma\{V_{sf}^G\} = 0{\cdot}6$; – × –, $\sigma\{V_{sf}^G\} = 0{\cdot}4$; –○–, $\sigma\{V_{sf}^G\} = 0{\cdot}2$.

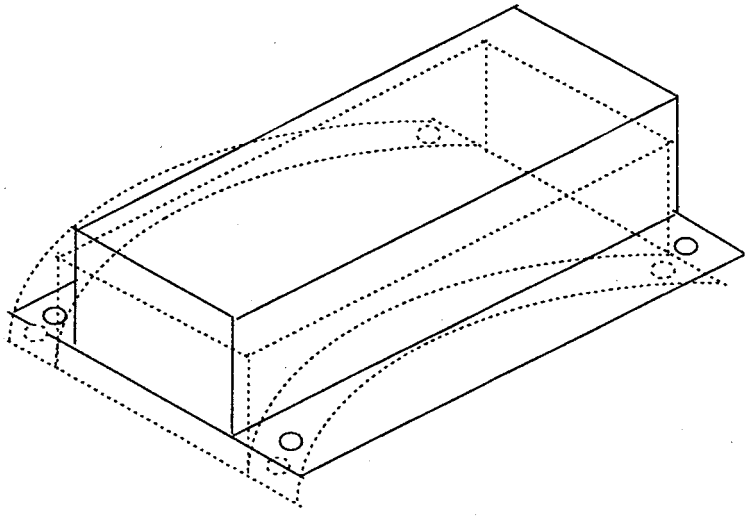

Figure 32. A source with a 2-flange base with stiffness-controlled behaviour.

Similar results were seen for both 3-flange and 4-flange models, so that for non-symmetric geometry, it is suggested that regardless of the total number of flanges involved the standard deviation of the force ratio resultant across a flange is realized by equation (31).

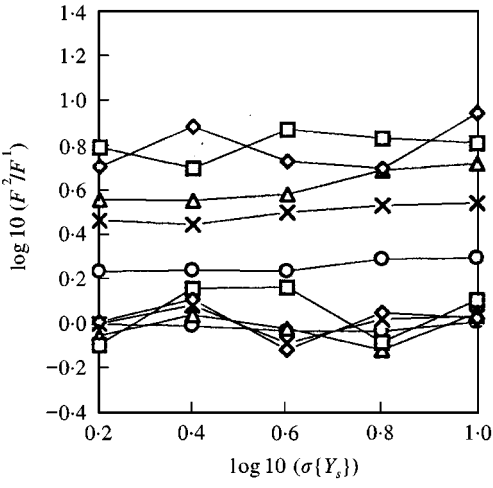

Figure 33. Force ratio statistics for symmetric stiffness-controlled source with 2-flanges. The x-axis represents the standard deviation of the grouped source mobilities. Their distribution is assumed to be log 10normal. The y-axis represents the distribution of the force ratios whereby the lower family of curves is the mean and the upper family of curves is the standard deviation. Again the distribution is assumed log 10normal. Each line on the figures is a different standard deviation of a free velocity log 10normal distribution: –◇– $\sigma\{V_{sf}^G\} = 1{\cdot}0$; –□–, $\sigma\{V_{sf}^G\} = 0{\cdot}8$; –△–, $\sigma\{V_{sf}^G\} = 0{\cdot}6$; – × –, $\sigma\{V_{sf}^G\} = 0{\cdot}4$; –○–, $\sigma\{V_{sf}^G\} = 0{\cdot}2$.

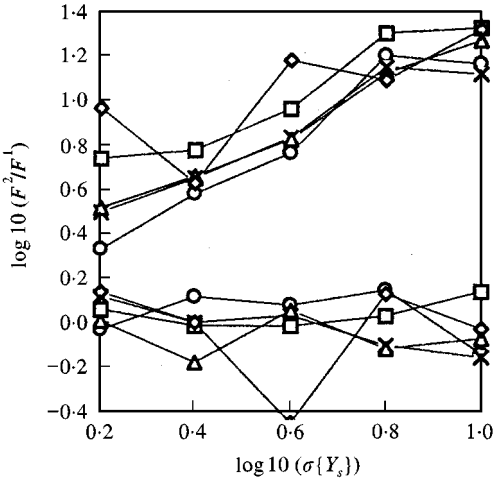

Figure 34. Force ratio statistics for non-symmetric stiffness-controlled source with 2-flanges. The x-axis represents the standard deviation of the grouped source mobilities. Their distribution is assumed to be log 10normal. The y-axis represents the distribution of the force ratios whereby the lower family of curves is the mean and the upper family of curves is the standard deviation. Again the distribution is assumed log 10normal. Each line on the figures is a different standard deviation of a free velocity log 10normal distribution: –◇– $\sigma\{V_{sf}^G\} = 1{\cdot}0$; –□–, $\sigma\{V_{sf}^G\} = 0{\cdot}8$; –△–, $\sigma\{V_{sf}^G\} = 0{\cdot}6$; – × –, $\sigma\{V_{sf}^G\} = 0{\cdot}4$; –○–, $\sigma\{V_{sf}^G\} = 0{\cdot}2$.

3.5.3. *Resonance-controlled source*

For a resonance-controlled source (see Figure 3) the statistics of (F^2/F^1) are shown in Figure 35. The result is common to that seen for a non-symmetric stiffness-controlled source where $\sigma\{(F^m/F^n)\}$ is dependent only upon $\sigma\{Y_s^G\}$ and the mean is consistently unity. Moreover, upon fitting a linear regression to the standard deviation, equation (31) is also again the result.

3.5.4. *Discussion*

In Table 4, the force ratio statistics for each of the mass, stiffness and resonance-controlled constant force sources are summarized.

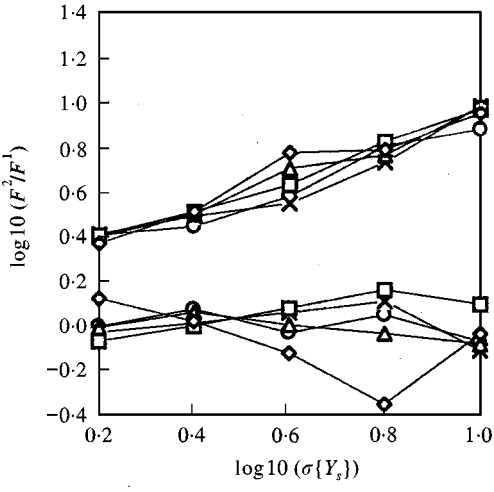

Figure 35. Force ratio statistics for resonance-controlled source. The x-axis represents the standard deviation of the grouped source mobilities. Their distribution is assumed to be log 10normal. The y-axis represents the distribution of the force ratios whereby the lower family of curves is the mean and the upper family of curves is the standard deviation. Again the distribution is assumed log 10normal. Each line on the figures is a different standard deviation of a free velocity log 10normal distribution: –◇– $\sigma\{V_{sf}^G\} = 1{\cdot}0$; –□–, $\sigma\{V_{sf}^G\} = 0{\cdot}8$; –△–, $\sigma\{V_{sf}^G\} = 0{\cdot}6$; – × –, $\sigma\{V_{sf}^G\} = 0{\cdot}4$; –○–, $\sigma\{V_{sf}^G\} = 0{\cdot}2$.

TABLE 4

Force ratio statistics for non-symmetrical CFS

	Source condition						
	Mass controlled Non-symmetric		Stiffness controlled Non-symmetric				
Description	High I_{xx} Low I_{yy}	Low I_{xx} High I_{yy}	2-flange	3-flange	4-flange	Plate	Resonance-controlled
Standard deviation of log 10normal distribution	$\sigma\{F^m/F^n\} \approx 0{\cdot}5 \times \sigma\{Y_s^G\} + 0{\cdot}5$		$\sigma\{F^m/F^n\} \approx 0{\cdot}7 \times \sigma\{Y_s^G\} + 0{\cdot}3$				
Mean	0						

An interesting feature is that for all cases where the source is non-symmetric the force ratio statistics are independent of the free velocity statistics. This is exciting, for if it translates to the situation of mobility matched source and receivers, the number of parameters determining the force ratio statistics in the general case is reduced from four to only three.

In view of equation (4) the difference between the formulation for the matched situation and for the CFS is the inclusion of the Y_r terms. Clearly though, providing both the receiver and source mobilities have a non-symmetric condition, the statistical "condition" of $(Y_s + Y_r)$ is as for (Y_s) inasmuch as the magnitude has a log 10 normal distribution while the phase has either a discretized or random-phase distribution (dependent upon the source and receiver conditions and which is dominant). It can be deduced therefore that for a source of non-symmetric geometry connected to a receiver of non-symmetric geometry, $\sigma\{(F^m/F^n)\}$ is also independent of $\sigma\{V_{sf}^G\}$ regardless of the mobility matching condition.

Hence, to reduce the volume of work, this result was introduced into the study of the force ratios for mobility matched source and receivers. Because of imperfections in design and manufacture it is suggested that such non-symmetric geometry is often found in practical situations and therefore this is not necessarily too restrictive.

3.6. FORCE RATIO MAGNITUDE DISTRIBUTION FOR MOBILITY MATCHED SOURCE AND RECEIVER

Each of the eight non-symmetric sources was paired with each of the three non-symmetric receivers to give a total of 24 distinct cases. In all cases, both $\sigma\{Y_s^G\}$ and $\sigma\{Y_r^G\}$ were, likewise for the CFS study, considered from 0·2 to 1 in increments of 0·2. The ratio of the receiver mobility mean to the source mobility mean, $E[Y_r^G]/E[Y_s^G]$, was considered from 10^0 to 10^{-5} in increments of $10^{0\cdot5}$.

For all, the mean of the force ratios approximated to unity so that the following results are concerned only with the standard deviation. Moreover, the statistics of one force ratio were found to be representative of all the force ratios so that only (F^2/F^1) is shown.

3.6.1. *Mass-controlled source*

For a mass-controlled source with high I_{yy}, low I_{xx} undergoing translational excitation and connected to a resonant-controlled receiver (see Figure 36) the standard deviation of (F^2/F^1) is shown in Figure 37 for the two extreme conditions of $\sigma\{Y_s^G\}$. On both figures, the x-axis represents the ratio $E[Y_r^G]/E[Y_s^G]$ and each line type a different case of $\sigma\{Y_r^G\}$.

Two regions are clearly apparent, which suggests that above and below approximately $E[Y_r^G]/E[Y_s^G] = 10^{-2}$ the matched and CFS situation exist respectively. For the case of $\sigma\{Y_s^G\} = 0\cdot2$ and the matched region, the standard deviation is seen to be dependent upon both $\sigma\{Y_s^G\}$ and $E[Y_r^G]/E[Y_s^G]$. Where $\sigma\{Y_s^G\} = 1\cdot0$ the influence of $\sigma\{Y_s^G\}$ does however diminish, this being, it is

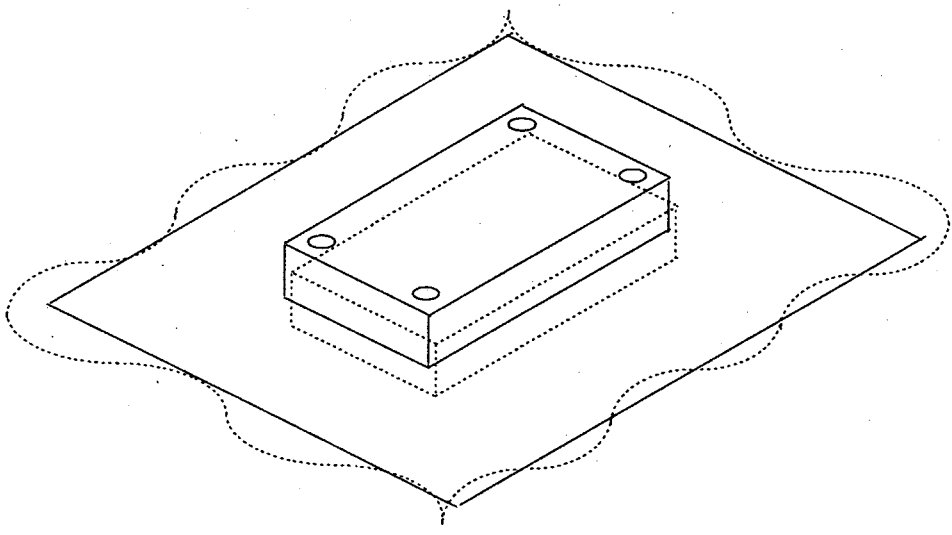

Figure 36. A source with mass-controlled behaviour and translational excitation attached to a receiver with resonance-controlled behaviour.

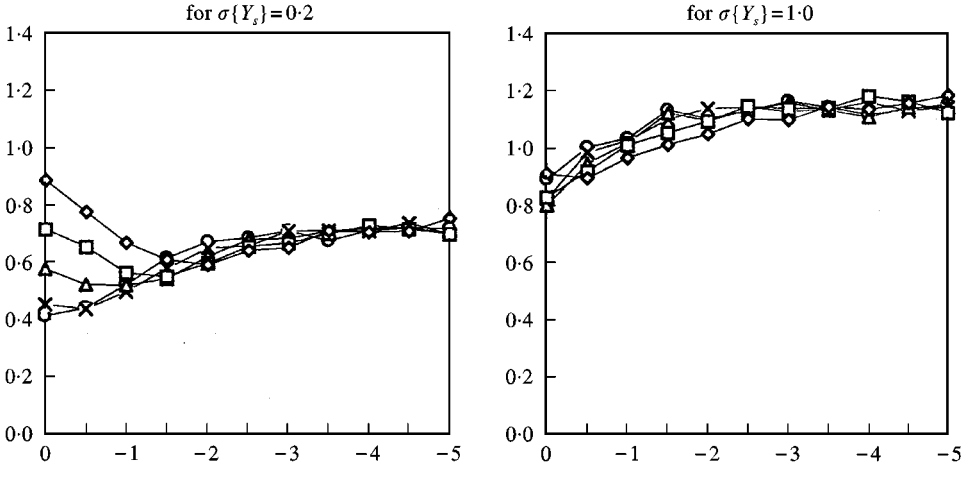

Figure 37. Standard deviation for a mass-controlled source, high I_{yy}, low I_{xx}, translational excitation, attached to a resonance-controlled receiver. The x-axis represents the ratio of the mean of the grouped receiver mobilities to the mean of the grouped source mobilities, i.e., $E[Y_r^G]/E[Y_s^G]$. Each of the grouped mobility distributions is assumed to be log 10normal and the scale is therefore logarithmic; i.e. -2 represents the condition where the source mean is 2 decades less than that of the receiver. The y-axis represents the standard deviation of force ratio. Again the distribution is assumed to be log 10normal. On each figure, each line represents a different standard deviation of receiver mobility distribution: –◇– $\sigma\{Y_r^G\} = 1{\cdot}0$; –□–, $\sigma\{Y_r^G\} = 0{\cdot}8$; –△–, $\sigma\{Y_r^G\} = 0{\cdot}6$; – × –, $\sigma\{Y_r^G\} = 0{\cdot}4$; –○–, $\sigma\{Y_r^G\} = 0{\cdot}2$.

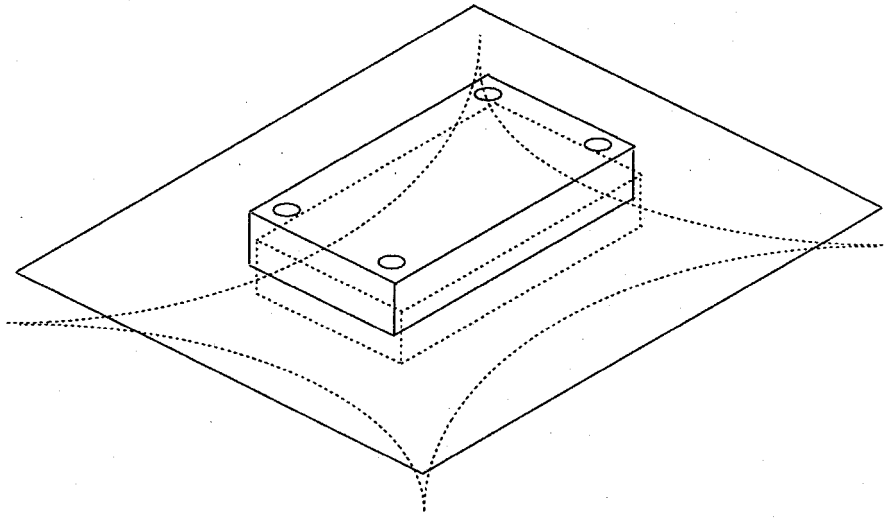

Figure 38. A source with mass-controlled behaviour and translational excitation attached to a receiver with stiffness-controlled behaviour.

suggested, a direct result of either Y_s or Y_r in the mobility sum $(Y_s + Y_r)$ of equation (4) being most dominant.

Similar results were seen when an infinite receiver was attached to the source. This can be expected since, with regard to the system description, only the phase allocated to the point mobilities: i.e., the statistical properties of the description remain the same.

However, when the mass is attached to a stiffness-controlled receiver (see Figure 38) the standard deviation increases in the matched region, see Figure 39. This indicates that with a stiffness-controlled receiver the source is more likely to undergo severe motion than with a resonant or infinite controlled receiver.

With regard to the influence of the excitation, reference can be made to the results of the CFS case where it was found that for a non-symmetric mass-controlled source, the form of the excitation (translational or rotational) had little influence upon the statistics of the force ratios. Since for all cases considered the receiver does not have a spatial condition associated with it (each mobility has an identical statistical state) the same can also be expected for the matched situation.

For the inter-relationship between the standard deviation and all of $\sigma\{Y_s^G\}$, $\sigma\{Y_r^G\}$ and $E[Y_r^G]/E[Y_s^G]$ an analytical expression can be achieved by assuming all the variables have a linear dependence.‡ Firstly, the relationships between $\sigma\{(F^m/F^n)\}$ and $\sigma\{Y_s^G\}, \sigma\{Y_r^G\}$ at both $E[Y_r^G]/E[Y_s^G] = 10^0$ and $E[Y_r^G]/E[Y_s^G] = 10^{-2}$ were obtained to produce Figures 40 and 41. The latter shows

‡Although compared to more significant curve-litting methods the linear approach will introduce larger discrepencies there, it is suggested, are limited with respect to the overall accuracy of the approach.

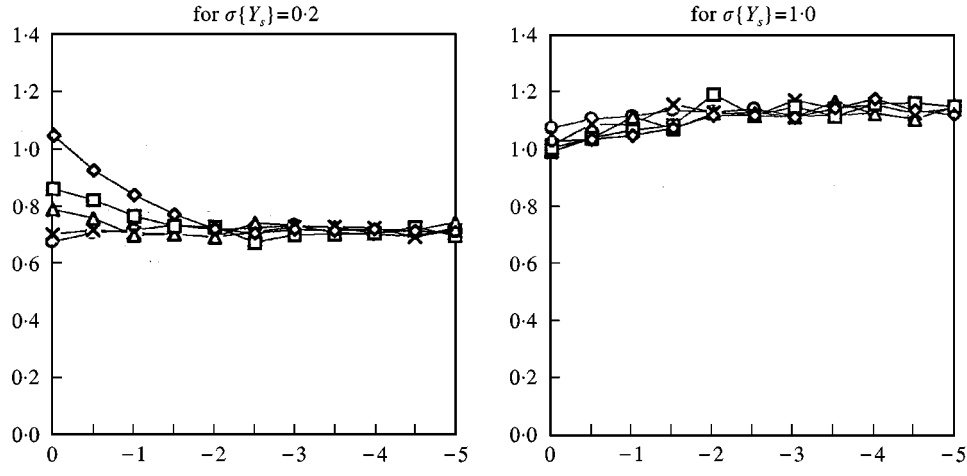

Figure 39. Standard deviation for a mass-controlled source, high I_{yy}, low I_{xx}, translational excitation, attached to a stiffness-controlled receiver. The x-axis represents the ratio of the mean of the grouped receiver mobilities to the mean of the grouped source mobilities, i.e., $E[Y_r^G]/E[Y_s^G]$. Each of the grouped mobility distributions is assumed to be log 10normal and the scale is therefore logarithmic; i.e. -2 represents the condition where the source mean is 2 decades less than that of the receiver. The y-axis represents the standard deviation of force ratio. Again the distribution is assumed to be log 10normal. On each figure, each line represents a different standard deviation of receiver mobility distribution: –◇– $\sigma\{Y_r^G\} = 1{\cdot}0$; –□–, $\sigma\{Y_r^G\} = 0{\cdot}8$; –△–, $\sigma\{Y_r^G\} = 0{\cdot}6$; – × –, $\sigma\{Y_r^G\} = 0{\cdot}4$; –○–, $\sigma\{Y_r^G\} = 0{\cdot}2$.

a CFS situation and the former a matched condition, wherefore equation (30) is suitable for Figure 41 whilst for Figure 40

$$\sigma\{(F^m/F^n)\} \approx 0{\cdot}7 \times (1 - \sigma\{Y_r^G\}) \times \sigma\{Y_s^G\} + 0{\cdot}8 \times \{Y_r^G\} \tag{32}$$

is appropriate. Combined, equations (30) and (32) give an approximate expression for the mass-controlled source matched to a resonance or infinite receiver,

$$\sigma\{(F^m/F^n)\} \approx \frac{2}{3}\frac{E[Y_r^G]}{E[Y_s^G]}[0{\cdot}7(1 - \sigma\{Y_r^G\})\sigma\{Y_s^G\} + 0{\cdot}8\sigma\{Y_r^G\} - 0{\cdot}5\sigma\{Y_s^G\} - 0{\cdot}6]$$
$$+ 0{\cdot}7(1 - \sigma\{Y_r^G\})\sigma\{Y_s^G\} + 0{\cdot}8\sigma\{Y_r^G\}, \tag{33}$$

for $10^0 \geqslant E[Y_r^G]/E[Y_s^G] > 10^{-2}$.

For a mass-controlled source matched to a stiffness-controlled receiver the expression is

$$\sigma\{(F^m/F^n)\} \approx \frac{2}{3}\frac{E[Y_r^G]}{E[Y_s^G]}[0{\cdot}5(1 - \sigma\{Y_r^G\})\sigma\{Y_s^G\} + \sqrt{\sigma\{Y_r^G\}} - 0{\cdot}5\sigma\{Y_s^G\} - 0{\cdot}6]$$
$$+ 0{\cdot}5(1 - \sigma\{Y_r^G\})\sigma\{Y_s^G\} + \sqrt{\sigma\{Y_r^G\}}, \tag{34}$$

for again $10^0 \geqslant E[Y_r^G]/E[Y_s^G] > 10^{-2}$.

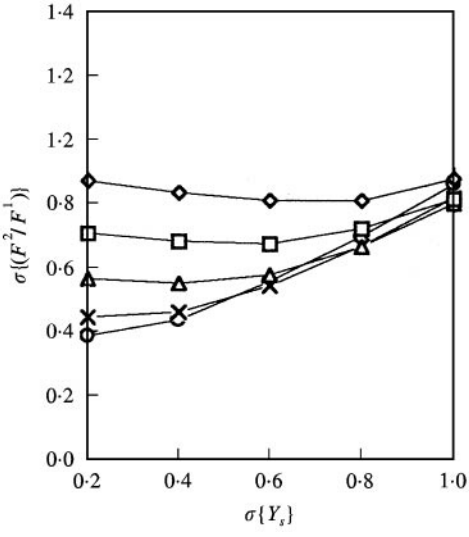

Figure 40. Standard deviation of F^m/F^n at $\log 10(E[Y_r^G]/E[Y_s^G]) = 0$ for a mass-controlled source attached to either a resonance or infinite receiver. The x-axis represents the ratio of the mean of the grouped receiver mobilities to the mean of the grouped source mobilities, i.e., $E[Y_r^G]/E[Y_s^G]$. Each of the grouped mobility distributions is assumed to be log 10normal and the scale is therefore logarithmic; i.e. -2 represents the condition where the source mean is 2 decades less than that of the receiver. The y-axis represents the standard deviation of force ratio. Again the distribution is assumed to be log 10normal. On each figure, each line represents a different standard deviation of receiver mobility distribution: –◇– $\sigma\{Y_r^G\} = 1{\cdot}0$; –□–, $\sigma\{Y_r^G\} = 0{\cdot}8$; –△–, $\sigma\{Y_r^G\} = 0{\cdot}6$; – × –, $\sigma\{Y_r^G\} = 0{\cdot}4$; –○–, $\sigma\{Y_r^G\} = 0{\cdot}2$.

3.6.2. *Stiffness-controlled source*

Where the source has a plate-like base and is attached to a resonance-controlled receiver the standard deviation is shown in Figure 42. Contrary to that seen with the mass-controlled source a similar result was also observed for both an infinite plate and stiffness-controlled receiver. This, as suggested, is resultant from the random phase of the free velocity for the stiffness-controlled source.

Comparable to the mass-controlled source, a CFS situation is realized for $E[Y_r^G]/E[Y_s^G] < 10^{-2}$ and a matched condition for $E[Y_r^G]/E[Y_s^G] > 10^{-2}$. Following a similar procedure to that used for the mass-controlled source, the relationship between the parameters in the matched region is

$$\sigma\{(F^m/F^n)\} \approx \frac{2}{3}\frac{E[Y_r^G]}{E[Y_s^G]}\,[0{\cdot}7(1-\sigma\{Y_r^G\})\sigma\{Y_s^G\} + 0{\cdot}8\sqrt{\sigma\{Y_r^G\}} - 0{\cdot}7\sigma\{Y_s^G\} - 0{\cdot}3]$$
$$+ 0{\cdot}7(1-\sigma\{Y_r^G\})\sigma\{Y_s^G\} + 0{\cdot}8\sqrt{\sigma\{Y_r^G\}}. \tag{35}$$

For a 2-flange stiffness-controlled source attached to a resonant receiver, the standard deviation is shown in Figure 43. For low values of $\sigma\{Y_s^G\}$ the statistics are similar to those observed for the plate-like base. However, in the matched region and when $\sigma\{Y_s^G\}$ is large the standard deviation is more sensitive to $\sigma\{Y_s^G\}$. That similar results were obtained when the source was either a 3- or 4-flange model and when the receiver was either stiffness controlled or an infinite plate means the

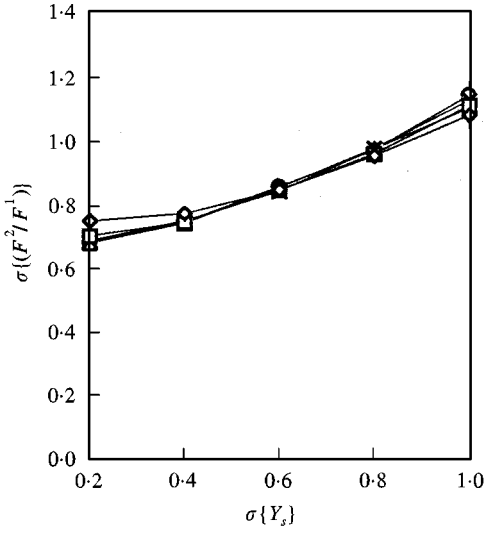

Figure 41. Standard deviation of F^m/F^n at log $10(E[Y_r^G]/E[Y_s^G]) = 2$ for a mass-controlled source attached to either a resonance or infinite receiver. The x-axis represents the ratio of the mean of the grouped receiver mobilities to the mean of the grouped source mobilities, i.e., $E[Y_r^G]/E[Y_s^G]$. Each of the grouped mobility distributions is assumed to be log 10normal and the scale is therefore logarithmic; i.e. -2 represents the condition where the source mean is 2 decades less than that of the receiver. The y-axis represents the standard deviation of force ratio. Again the distribution is assumed to be log 10normal. On each figure, each line represents a different standard deviation of receiver mobility distribution: $-\diamond-$ $\sigma\{Y_r^G\} = 1{\cdot}0$; $-\square-$, $\sigma\{Y_r^G\} = 0{\cdot}8$; $-\triangle-$, $\sigma\{Y_r^G\} = 0{\cdot}6$; $-\times-$, $\sigma\{Y_r^G\} = 0{\cdot}4$; $-\bigcirc-$, $\sigma\{Y_r^G\} = 0{\cdot}2$.

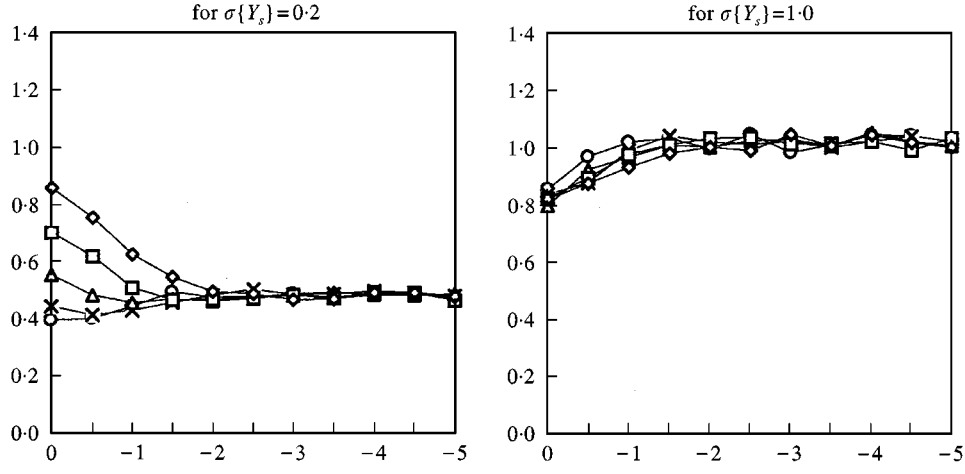

Figure 42. Standard deviation for a stiffness-controlled source with plate-like base, attached to a resonance-controlled receiver. The x-axis represents the ratio of the mean of the grouped receiver mobilities to the mean of the grouped source mobilities, i.e., $E[Y_r^G]/E[Y_s^G]$. Each of the grouped mobility distributions is assumed to be log 10normal and the scale is therefore logarithmic; i.e. -2 represents the condition where the source mean is 2 decades less than that of the receiver. The y-axis represents the standard deviation of force ratio. Again the distribution is assumed to be log 10normal. On each figure, each line represents a different standard deviation of receiver mobility distribution: $-\diamond-$ $\sigma\{Y_r^G\} = 1{\cdot}0$; $-\square-$, $\sigma\{Y_r^G\} = 0{\cdot}8$; $-\triangle-$, $\sigma\{Y_r^G\} = 0{\cdot}6$; $-\times-$, $\sigma\{Y_r^G\} = 0{\cdot}4$; $-\bigcirc-$, $\sigma\{Y_r^G\} = 0{\cdot}2$.

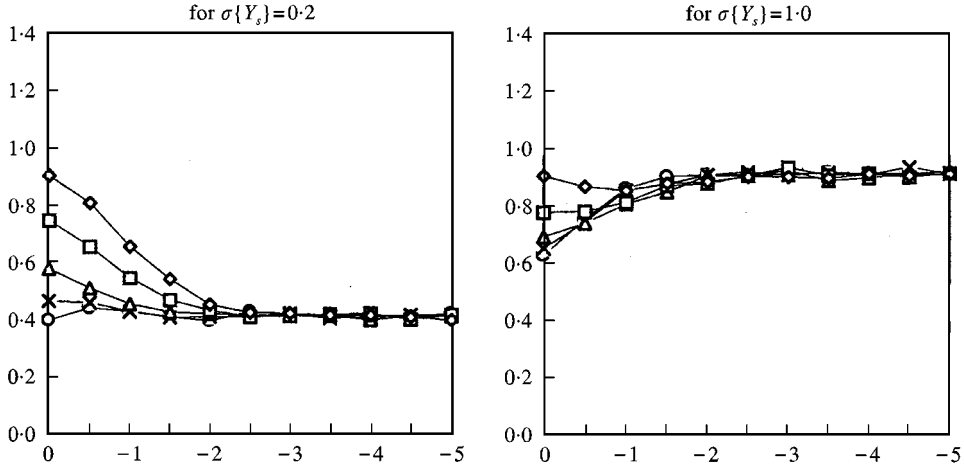

Figure 43. Standard deviation for a stiffness-controlled source with 2-flanges, attached to a resonance-controlled receiver. The x-axis represents the ratio of the mean of the grouped receiver mobilities to the mean of the grouped source mobilities, i.e., $E[Y_r^G]/E[Y_s^G]$. Each of the grouped mobility distributions is assumed to be log 10normal and the scale is therefore logarithmic; i.e. -2 represents the condition where the source mean is 2 decades less than that of the receiver. The y-axis represents the standard deviation of force ratio. Again the distribution is assumed to be log 10normal. On each figure, each line represents a different standard deviation of receiver mobility distribution: –◇– $\sigma\{Y_r^G\} = 1{\cdot}0$; –□–, $\sigma\{Y_r^G\} = 0{\cdot}8$; –△–, $\sigma\{Y_r^G\} = 0{\cdot}6$; – × –, $\sigma\{Y_r^G\} = 0{\cdot}4$; –○–, $\sigma\{Y_r^G\} = 0{\cdot}2$.

expression derived from the results

$$\sigma\{(F^m/F^n)\} \approx \frac{2}{3}\frac{E[Y_r^G]}{E[Y_s^G]}[0{\cdot}4(1-\sigma\{Y_r^G\})\sigma\{Y_s^G\} + 0{\cdot}8\sqrt{\sigma\{Y_r^G\}} - 0{\cdot}7\sigma\{Y_s^G\} - 0{\cdot}3]$$

$$+ 0{\cdot}4(1-\sigma\{Y_r^G\})\sigma\{Y_s^G\} + 0{\cdot}8\sqrt{\sigma\{Y_r^G\}}, \tag{36}$$

is suitable for all in the matched region.

3.6.3. *Resonance-controlled source*

For a resonance-controlled source attached to a resonance-controlled receiver, the result procured is shown in Figure 44. Similar results were seen when the receiver was either stiffness or infinite controlled. Moreover, the relationship devised between the parameters is similar to that of a stiffness-controlled source with a plate-like base, i.e., equation (35).

The results are summarized in Table 5.

4. CONCLUDING REMARKS

In view of the source descriptor and coupling function formulation, both an analytical and a statistical study has been undertaken with regard to estimating the force ratios in multi-point-connected source–receiver systems.

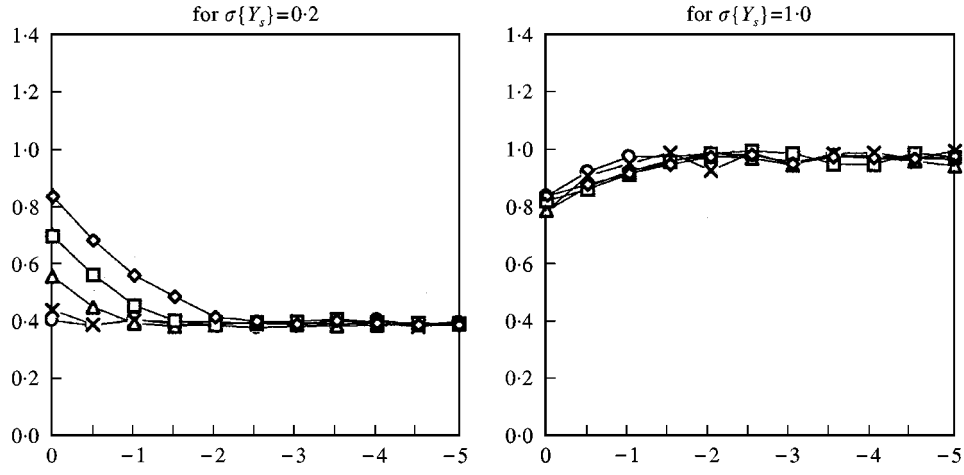

Figure 44. Standard deviation for a resonance-controlled source, attached to a resonance-controlled receiver. The x-axis represents the ratio of the mean of the grouped receiver mobilities to the mean of the grouped source mobilities, i.e., $E[Y_r^G]/E[Y_s^G]$. Each of the grouped mobility distributions is assumed to be log 10normal and the scale is therefore logarithmic; i.e. -2 represents the condition where the source mean is 2 decades less than that of the receiver. The y-axis represents the standard deviation of force ratio. Again the distribution is assumed to be log 10normal. On each figure, each line represents a different standard deviation of receiver mobility distribution: –◇– $\sigma\{Y_r^G\} = 1{\cdot}0$; –□–, $\sigma\{Y_r^G\} = 0{\cdot}8$; –△–, $\sigma\{Y_r^G\} = 0{\cdot}6$; – × –, $\sigma\{Y_r^G\} = 0{\cdot}4$; –○–, $\sigma\{Y_r^G\} = 0{\cdot}2$.

For the analytical study, estimate solutions based upon both iteration and matrix inversion methods were considered. However, all schemes failed when the magnitudes of the transfer mobilities approached those of the point mobilities. Since this condition is common for resonance-controlled sources, and can also occur when the source is either mass or, with a plate-like base, stiffness controlled, these approaches are considered unreliable. The revealed sensitivity of the force ratios to all the mobilities is also important, since it suggests that any analytical method developed to obtain the force ratios would have to be based upon highly accurate data.

In the statistical study, grouped mobility functions were introduced. To obtain these, the mobilities (point and transfer) of a structure were considered as a population, for which the statistical properties were used to define the grouped mobility function. A log 10 normal distribution was suggested for the magnitude while for the phase, a uniform distribution was suggested provided the behaviour was resonance controlled. For mass- or stiffness-controlled behaviour the phase is deterministic and hence its distribution was not considered.

Grouped functions were also defined for the free velocities.

Based upon these grouped functions, a number of source–receiver systems were defined and a methodology based upon a Monte Carlo approach was used to determine the statistics of the force ratios.

For all the systems, the force ratio had a log 10 normal distribution with a mean of unity.

TABLE 5

Force ratio statistics for mobility matched source and receiver

Description	Source condition non-symmetric / Receiver condition non-symmetric	Mass-controlled			Stiffness-controlled flange-like base			Stiffness-controlled plate-like base			Resonance-controlled		
		Stiffness controlled	Resonance controlled	Infinite plate	Stiffness controlled	Resonance controlled	Infinite plate	Stiffness controlled	Resonance controlled	Infinite plate	Stiffness controlled	Resonance controlled	Infinite plate
Standard deviation of log 10normal distribution for $0 < \mathrm{E}[Y_r^G]/E[Y_s^G] < -2$		Equation (34)	Equation (33)		Equation (36)			Equation (35)					
Mean							0						

For a constant force situation and where the source had symmetrical geometry the standard deviation of the distribution was dependent upon whether the source was mass or stiffness controlled and also upon both the grouped mobility function and grouped free velocity function. Due to the imprecise nature of the sampled results, empirical relationships between the variables could not be determined. For non-symmetrical geometry, the force ratios were independent of the grouped free velocity function. Empirical relationships between the parameters were derived; for a mass-controlled source the standard deviation of the force ratio magnitude distribution is given by equation (30) and for both stiffness- and resonant- controlled sources it is given by equation (31).

For the matched condition, only non-symmetric sources were studied. For the CFS, the standard deviation of the force ratios was deduced to be independent of the grouped free velocity function. As regards the grouped mobility functions, the standard deviation of the force ratios was dependent upon which had the largest standard deviation. For a mass-controlled source there was also some dependence upon the phase condition of the receiver such that equation (34) was applicable for a stiffness-controlled receiver and equation (33) applicable for both a resonance and infinite plate receiver. If the source was stiffness controlled with a flange-like base equation (36) was applicable while, if the source was either stiffness controlled or resonance controlled with a plate-like base equation (35) was applicable.

Thus, a methodology has been developed through which statistical estimates of the force ratios in multi-point-connected source–receiver systems can be obtained. It is this that provides a step towards overcoming the inherent problem of the source descriptor and coupling function formulation for systems. Application of the expressions developed obtain statistical estimates of the source descriptor, coupling function and transmitted power will be reported in forthcoming paper.

ACKNOWLEDGMENTS

This study was financially supported by the Engineering and Physical Sciences Research Council, U.K. The support is gratefully acknowledged.

REFERENCES

1. R. A. Fulford and B. M. Gibbs 1997 *Journal of Sound and Vibration* **204**, 659–677. Structure-borne sound power and source characterisation in multi-point-connected systems. Part 1: case studies for assumed force distribution.
2. J. M. Mondot and B. A. T. Petersson 1987 *Journal of Sound and Vibration* **114**, 507–518. Characterisation of structure-borne sound sources: the source descriptor and coupling function.
3. R. A. Fulford and B. M. Gibbs 1999 *Journal of Sound and Vibration* **220**(1), 203–224. Structure-borne sound power and source characterisation in multi-point-connected systems. Part 2: general relationships for mobility functions and free velocities.

4. B. A. T. Petersson and B. M. Gibbs 1993 *Journal of Sound and Vibration* **168**, 157–176. Use of the source descriptor concept in studies of multi-point and multi-directional vibrational sources.
5. F. J. Fahy and M. E. Westcott 1978 *Journal of Sound and Vibration* **57**, 101–129. Measurement of floor mobility at low frequencies in some buildings with long floor spans.
6. S. C. Lennox and M. Chadwick 1985 *Mathematics for Engineers and Applied Scientists*. London: Heinemann Educational Books.
7. L. Cremer, M. Heckl and E. Ungar 1973 *Structure-Borne Sound*. Berlin: Springer-Verlag, second edition.
8. *ANSI* S2.31-1979, S2-32-1982. Methods for the experimental determination of mechanical mobility: Parts I and II.
9. R. H. Lyon 1975 *Statistical Energy Analysis of Dynamical Systems*. Cambridge, MA: The MIT Press.
10. C. Chatfield 1978 *Statistics for Technology*. New York: Halstead Press.
11. M. Kendall and A. Stuart, 1977 *The Advanced Theory of Statistics. Volume* 1: *Distribution Theory* (*fourth edition*). London: Charles Griffin and Company Limited.
12. N. Dimitris and P. E. Chorafas 1960 *Statistical Process and Reliability Engineering*. New York: Van Nostrand.
13. R. A. Fulford 1995 *Ph.D. Thesis*, *University of Liverpool*. Structure-borne sound power and source characterisation in multi-point-connected systems.

APPENDIX: SYMBOLS AND NOTATION

Cf	coupling function
F	force
S	source descriptor
V_{sf}	free velocity
Y	mobility
k	radius of gyration
m	mass
x	position
ε	ratio
ω	angular frequency
ψ	eigenmode
η	loss factor
$E[\ ]$	mean
$\mathrm{Im}\{\ \}$	imaginary component
$\mathrm{Re}\{\ \}$	real component
$e\{\ \}$	variable parameter
$\sigma\{\ \}$	standard deviation
$\theta\{\ \}$	phase angle

Indices

G	grouped function
i	direction
it	iteration number
j	direction
m	location
n	location
$norm$	normalized quantity
pt	point

r	receiver
s	source
t	equation component
tr	transfer
u	equation component
Σ	effective mobility

Notation

*	complex conjugate